Climate Change and the Middle Atmosphere. Part IV: Ozone Response to Doubled CO_2

DREW T. SHINDELL AND DAVID RIND

NASA/Goddard Institute for Space Studies and Center for Climate Systems Research, Columbia University, New York, New York

PATRICK LONERGAN

Science Systems and Applications, New York, New York

(Manuscript received 5 November 1996, in final form 9 May 1997)

ABSTRACT

Parameterized stratospheric ozone photochemistry has been included in the Goddard Institute for Space Studies (GISS) GCM to investigate the coupling between chemistry and climate change for the doubled CO_2 climate. The chemical ozone response is of opposite sign to temperature changes, so that radiative cooling in the upper stratosphere results in increased ozone, while warming reduces ozone in the lower stratosphere. The increased overhead column reduces the amount of UV reaching the lower stratosphere, resulting in further ozone decreases there. Changes of up to 15% are seen, including both photochemistry and transport. Good agreement is found between the authors' results and those in other models for tropical latitudes where the stratospheric temperature responses are similar. However, in the extratropics, there are large differences between present results and those of the other models due to differences in tropospheric warming and tropospheric forcing of the stratospheric residual circulation. A net decrease in column ozone at midlatitudes is seen in this climate model, in contrast to the other models that showed an increase in column ozone everywhere. These ozone reductions lead to an increase of 10% in UV radiation reaching the surface at northern midlatitudes. The authors find significantly less of an increase in the high-latitude ozone column than in the other models.

When parameterized heterogeneous chemistry on polar stratospheric clouds is also included, while maintaining current chlorine loading, it is found that the Antarctic ozone hole becomes significantly larger and of longer duration. In addition, an ozone hole of approximately half the depth in percent of the current Antarctic ozone hole forms in the Arctic due to both chemistry and transport changes resulting from a reduction of sudden warmings seen in the doubled CO_2 atmosphere.

1. Introduction

Ozone changes will take place in response to increasing greenhouse gas concentrations in the earth's atmosphere. These changes could have significant impacts on climate change and on the amount of harmful UV radiation reaching the earth's surface, since ozone plays a major role in atmospheric radiation and dynamics. Increasing rates of carbon dioxide emissions into the atmosphere are now well documented (e.g., Keeling et al. 1989). The long-term consequences of the buildup of greenhouse gases in the atmosphere can best be assessed with general circulation models (GCMs). These models have indicated that surface temperatures are likely to rise by several degrees over the coming decades in response to predicted greenhouse gas emissions, the phenomenon known as ''global warming.'' For a doubling of CO_2, a standard benchmark test, the surface temperature of the earth is predicted to increase by 1.5°–5°C (e.g., Manabe and Wetherald 1975; Rind 1987; Intergovernmental Panel on Climate Change 1995). Accompanying the tropospheric warming should be stratospheric cooling (e.g., Fels et al. 1980; Rind et al. 1990).

These temperature changes will have an impact on ozone chemistry in the stratosphere, which will feed back on temperature, since ozone itself is an absorbing gas. Changes in stratospheric ozone will also alter the radiation field at lower levels, affecting dynamics and chemistry down into the troposphere. Since the inclusion of complete chemistry in a long-term GCM suitable for climate modeling is prohibitively expensive computationally, GCM experiments have so far generally neglected any chemical response to doubled CO_2 ($2 \times CO_2$). The response of stratospheric ozone to a $2 \times CO_2$ loading of the atmosphere has been investigated in stratospheric chemistry models, however. These models predict increases in total column ozone of up to ~8%, with localized increases of up to ~30% (Brasseur et al. 1990; Pitari et al. 1992; Schneider et al. 1993). However, these

Corresponding author address: Dr. Drew T. Shindell, NASA/GISS, 2880 Broadway, New York, NY 10025.
E-mail: dshindell@giss.nasa.gov

models all used prescribed conditions in the troposphere. Additionally, a $2 \times CO_2$ simulation has been performed with the Météo-France climate model using prescribed sea surface temperature changes (Mahfouf et al. 1994) and a transient buildup of carbon dioxide.

We have used parameterized stratospheric chemistry to model the equilibrium chemical response of stratospheric ozone to $2 \times CO_2$ in the Goddard Institute for Space Studies (GISS) GCM. The parameterized chemistry is computationally rapid enough to permit long-term climate simulations to be carried out with this coupled chemistry–climate GCM. Unlike the stratospheric chemistry models, this coupled model explicitly calculates $2 \times CO_2$-induced changes in tropospheric temperatures and changes in residual circulation due to tropospheric warming. In contrast to the Météo-France climate model, sea surface temperatures in the GISS GCM are allowed to equilibrate with the $2 \times CO_2$ atmosphere, which also affects the tropospheric response. Through temperature and circulation, the tropospheric response exerts a significant influence on the stratosphere in our climate model. In addition to the online calculations of photochemical ozone changes, we have calculated off-line the ozone transport changes in the $2 \times CO_2$ atmosphere. In this paper, we present the photochemical and transport ozone responses to $2 \times CO_2$ in our model, compare the results with those of the other models, and discuss the implications of the ozone changes calculated in our model for global warming predictions and surface UV flux.

2. Parameterization of ozone photochemistry

In order to include the effects of ozone chemistry in $2 \times CO_2$ simulations, we have derived parameterizations of the dependence of ozone on temperature and the local radiation field, which are included on-line in the GCM. The ozone responds initially to changes in temperature between the $2 \times CO_2$ run and the control run ($1 \times CO_2$). Once ozone has changed, the altered profile then absorbs a different amount of radiation, feeding back on the local temperature by altering the solar and thermal heating rates, as well as changing the radiation field above and below the region of ozone change. Throughout the stratosphere, from 200 to 0.1 mb, ozone in the GCM both responds photochemically to and directly affects temperature and the radiation field, both of which then alter dynamics. The parameterizations of ozone response to changes in temperature and in the radiation field were derived using a quasi two-dimensional approach. Photochemical calculations were done using the one-dimensional model of Shindell and de Zafra (1996), which contains a full set of chemical and photolytic reactions important in the stratosphere (see appendix). Rate constants and photolysis cross sections were primarily from the National Aeronautics and Space Administration (NASA) Jet Propulsion Laboratory (JPL) 1994 evaluation (DeMore et al. 1994), with the exceptions noted in Shindell and de Zafra (1996). The model was run with the inclusion of climatological values of vertical and meridional transport, derived from the transport terms calculated in the GCM, which especially impacts the ozone and NO_x/NO_y distributions. As shown in Fig. 1, this quasi two-dimensional approach reproduces the observed annual variation seen in ground-based and satellite data quite well for ozone and does a reasonable job for the reactive ozone depleting species such as the NO_x family, given that the uncertainties in the NO_x measurements are roughly a factor of 2 [observations as given in World Meteorological Organization (1985), and SAGE II data]. Comparisons with longer-lived NO_y species, such as the HNO_3 shown in Fig. 1, are also quite good. Observations of the short-lived HO_x species to date have even larger uncertainties than the NO_x measurements and so do not allow a meaningful comparison of observed and modeled seasonal cycles. Deviations from the equilibrium annual cycle of ozone due to temperature changes and due to changes in overhead ozone column were then derived independently at each latitude and altitude.

Throughout the middle and lower stratosphere, cooling slows down the rate of the chemical reactions that deplete odd oxygen [$O_x = O + O(^1D) + O_3$]. Odd oxygen production at a given location is only very weakly temperature dependent, occurring primarily through the photolysis of molecular oxygen into atomic oxygen. A decrease in temperature therefore leads to a net increase in the amount of odd oxygen, and hence ozone, present.

The temperature sensitivity of the odd oxygen loss processes varies with the reactive family involved. In our model, the O_x and HO_x families exhibit the largest sensitivities, while the NO_x family is the least sensitive. These trends are in general agreement with the model results given in World Meteorological Organization (1985), though these used older values of reaction rate constants and photolysis cross sections. The overall odd oxygen response, shown in the left panel of Fig. 2, is therefore largest in the lower and upper stratosphere, where HO_x and O_x are, respectively, the dominant contributors to O_x loss. The response shows a local minimum near 32-km altitude, where NO_x chemistry dominates. Over a 10°C range of temperature change, that seen in previous doubled CO_2 runs (Rind et al. 1990), the response is fairly linear. The small nonlinearity exhibited here has been included in the parameterizations.

The amount of ozone present at a particular depth is also a function of the amount of shortwave radiation penetrating to that depth. Since ozone itself is a shortwave absorber, the amount of ozone at a given altitude depends on the column of ozone above that altitude. The right panel of Fig. 2 shows the percent change in ozone concentration per percent increase in overhead column calculated in the quasi two-dimensional model using spherical geometry with a delta-Eddington technique for radiative transfer. The amount of ozone change

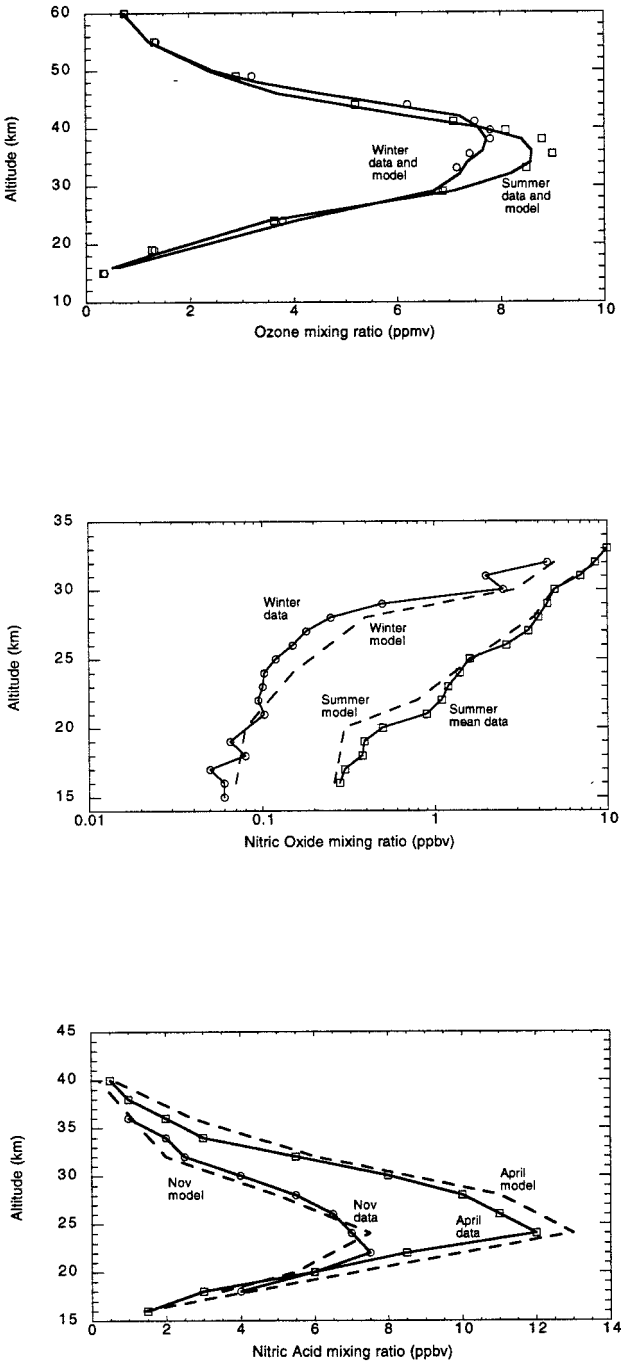

FIG. 1. Comparison of observed seasonal variability with that produced in the quasi two-dimensional model. The first panel compares ozone results throughout the stratosphere for 30°N. The second panel shows nitric oxide results in the mid- and lower stratosphere for 50°–51°N (note that the uncertainty on the NO measurements is roughly a factor of two), while the third shows nitric acid for 50°S. Data taken from World Meteorological Organization (1985) supplemented with SAGE II ozone profile data in the lower stratosphere and from Roche et al. (1994) for nitric acid.

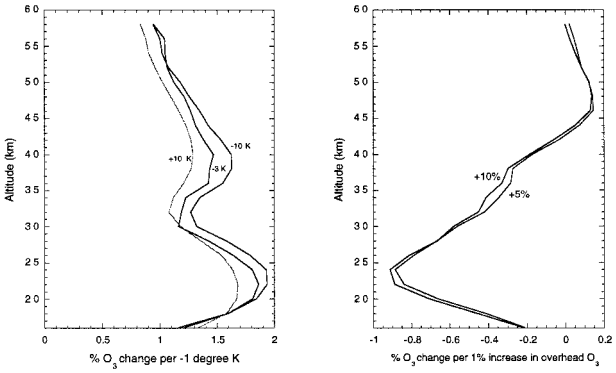

FIG. 2. The left panel shows the response of ozone to a temperature change throughout the stratosphere. The response is nearly, though not completely, linear over the expected temperature range. This nonlinearity is included in the parameterization. The right panel shows the response of ozone to an increase in the overhead ozone column. The response is very linear. Both responses are given at 30°N, after equilibration.

was again derived independently at each altitude. In addition, vertical eddy diffusion was shut off for ozone to remove any influence of changes in neighboring layers. As seen in Fig. 2, the final response was quite linear over the expected range of ozone changes.

The parameterizations of ozone response to temperature and overhead ozone changes were derived at 15° intervals in latitude. The temperature sensitivity of ozone chemistry increases slightly with latitude, as the weakly temperature-dependent production of ozone from photolysis of oxygen plays a less significant role compared to the more strongly temperature-dependent chemical reactions. The opposite is true for sensitivity to overhead ozone column, however, as the photolysis of NO_2 becomes a more important source of O_x production than the photolysis of O_2 at higher latitudes. Since NO_2 is photolyzed by longer wavelengths that are not absorbed as efficiently by ozone, as takes place down into the troposphere, the overall O_x abundance is less sensitive to the overhead column amount at high latitudes. The resulting latitude versus altitude arrays of ozone response to changing temperature and overhead ozone column were included as functional relationships in the GCM. For example, at 25-km altitude, 30°N, ozone decreases linearly at a rate of -0.8% $(1\%)^{-1}$ increase in the overhead ozone column and changes by $[(-1.7 + \Delta T/100) \times \Delta T]\%$ for a temperature change of ΔT (as shown in Fig. 2). Changes are applied daily with a timescale inversely proportional to the lifetime of ozone at a given altitude, that is, $\Delta O_3 = \Delta O_3/\tau$. At high altitudes where ozone's lifetime is less than one day, changes are instantaneous. At high latitudes during the polar night, the prevailing ozone responses at polar sunset were ''frozen in,'' under the assumption that ozone photochemistry is suspended. Climatological variation is maintained throughout this period for the affected regions, however.

The parameterized ozone photochemistry was included on-line in the 23-layer version of the GISS GCM. This model has 8° × 10° resolution, with the vertical layers extending from the surface to 85 km. The GISS GCM is a primitive equation model that includes parameterized gravity waves (Rind et al. 1988a, 1988b). The GCM was run in an equilibrium $2 \times CO_2$ experiment, including the chemical response of ozone. A detailed description can be found in Rind et al. (1998), a companion paper to this, hereafter referred to as Part III. Changes in ozone transport induced by the photochemical changes and by the circulation changes were calculated offline for these experiments. We focus initially on the photochemical response of ozone to $2 \times CO_2$ without including the effects of polar heterogeneous chemistry or transport.

3. Ozone photochemical response to $2 \times CO_2$ in the coupled model

Sea surface temperatures require ~25 yr to equilibrate with doubled atmospheric CO_2 in the GISS GCM. We performed a 50-yr control run and a 50-yr run incorporating the ozone parameterizations discussed above in which the sea surface temperatures were allowed to adjust from current values to equilibrium with the $2 \times CO_2$ atmosphere. Additionally, the model was run for 20 yr starting from year 25 of an earlier $2 \times CO_2$ run performed without chemistry. We concentrate first on the results of the 50-yr chemistry run. In general, we show results and differences averaged over the last 20 yr of the 50-yr runs, when the sea surface temperatures have fully equilibrated with the doubled atmospheric CO_2.

The zonal mean temperature response to $2 \times CO_2$ is shown in Fig. 3 ($2 \times CO_2$ minus control). These temperature changes include a negative feedback from chemically changing ozone. The dynamical and radiative changes that lead to this temperature response to $2 \times CO_2$ are detailed in Part III. We restrict ourselves here to discussing the impact of $2 \times CO_2$ upon ozone. The primary features of the temperature response are the large cooling in the upper stratosphere and the large warming in the upper troposphere. Since temperature has a negative feedback upon ozone photochemistry, these changes lead to increased ozone at high altitudes and decreased ozone lower down, as shown in Fig. 4 in percentage and in Fig. 5 in Dobson units (DU) per kilometer of altitude.

Upper stratospheric ozone increases by up to 15%. The location and magnitude of the increase mirrors the CO_2-induced cooling. For example, the ozone increase at high southern latitudes is clearly largest from September through February, when the temperature decrease is also largest. In general, the upper stratospheric ozone response is dominated by the sensitivity of ozone photochemistry to temperature changes rather than to radiation changes. As shown in the right panel of Fig. 2, the ozone response to changes in the overhead column is fairly weak in the upper stratosphere. Since the density of the overhead column is small, it has little influence on the UV radiation passing through it. Above ~43-km altitude, an increase in the overhead ozone column actually leads to an increase in the amount of ozone present, as the photolytic destruction of ozone is reduced more than its production via oxygen photolysis, though the response is still quite weak. The ozone sensitivity to temperature is strongest around 36–41-km altitude (~5–1 mb), which is also where the temperature decrease in response to $2 \times CO_2$ is largest. It is no surprise then that the ozone increases in the upper stratosphere are greatest in that altitude region and are roughly proportional to the temperature decreases throughout the upper stratosphere.

Since there is more ozone in the upper stratosphere, ozone at lower altitudes responds to the reduction in radiation due to the increased overhead ozone as well as to the local CO_2-induced temperature changes. These two responses tend to balance each other at a point in the middle stratosphere just above the changeover from cooling to warming. For example, the ozone change over the equator during March–May (upper right panel of Fig. 4) is zero at ~45 mb. At this point, the decrease in chemical ozone loss rates due to a 2°C cooling is exactly compensated for by the decrease in photochemical ozone production due to the increased overhead column's greater absorption of radiation. In the lower stratosphere, ozone decreases significantly at equatorial and midlatitudes. A local warming and the reduction in local radiation combine to cause large reductions in the amount of ozone there, with ozone response to temperature change dominating at the lowest altitudes where strong warming occurs in the GCM. The greatest ozone decreases are at midlatitudes, where the CO_2-induced warming extends to higher altitudes than near the equator. Though the largest percentage changes are in the upper stratosphere, the largest changes in ozone amounts are here, where the majority of ozone is located, as seen in Fig. 5. The lifetime of ozone is fairly long in the lower stratosphere, so that transport changes will also be significant there, as discussed below.

In the polar regions, the ozone response is somewhat more complex. Changes in residual circulation and wave propagation induced by the doubling of CO_2 (see Part III) lead to increased transport of heat into the high-altitude polar regions. This partially compensates for the CO_2-induced radiative cooling, resulting in a smaller amount of cooling there compared to the upper stratosphere at lower latitudes. At northern high latitudes, the temperature changes are very small in the upper stratosphere (except June–August), with CO_2-induced cooling and increased dynamical heating roughly in balance. The resulting ozone changes are also small. Due to the increased overhead ozone and slight warmings in the middle stratosphere, there is a reduction of ozone in the middle and lower stratosphere in the northern polar re-

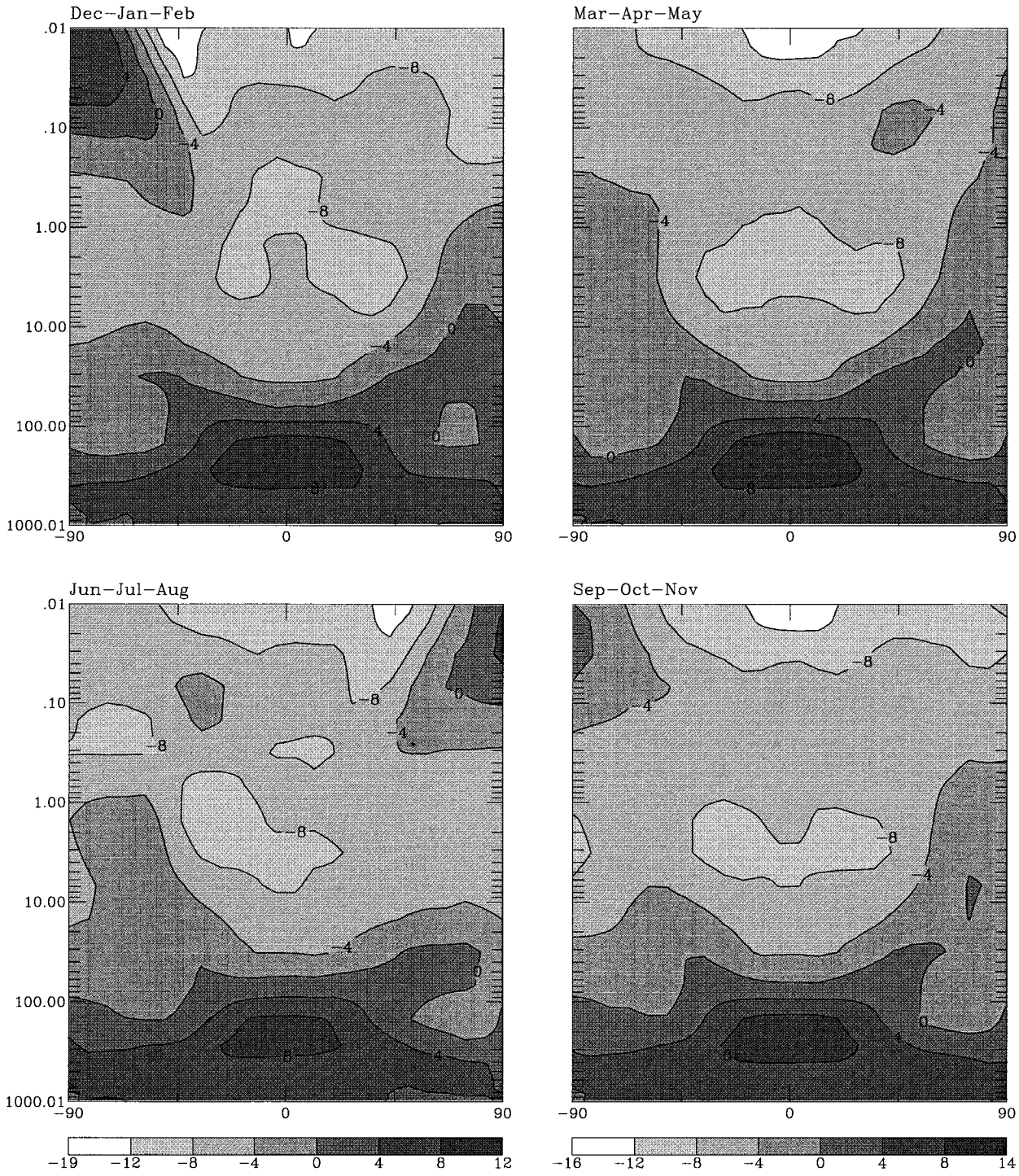

FIG. 3. Seasonal temperature change due to doubled atmospheric CO_2 including ozone chemical feedback (ozone's response to the CO_2-induced temperature changes). The difference in °C between zonal average temperature in the doubled CO_2 and the standard CO_2 runs is shown, averaged over the last 20 yr of a 50-yr run performed for each CO_2 loading. The vertical axis is pressure in millibars, while the horizontal is latitude.

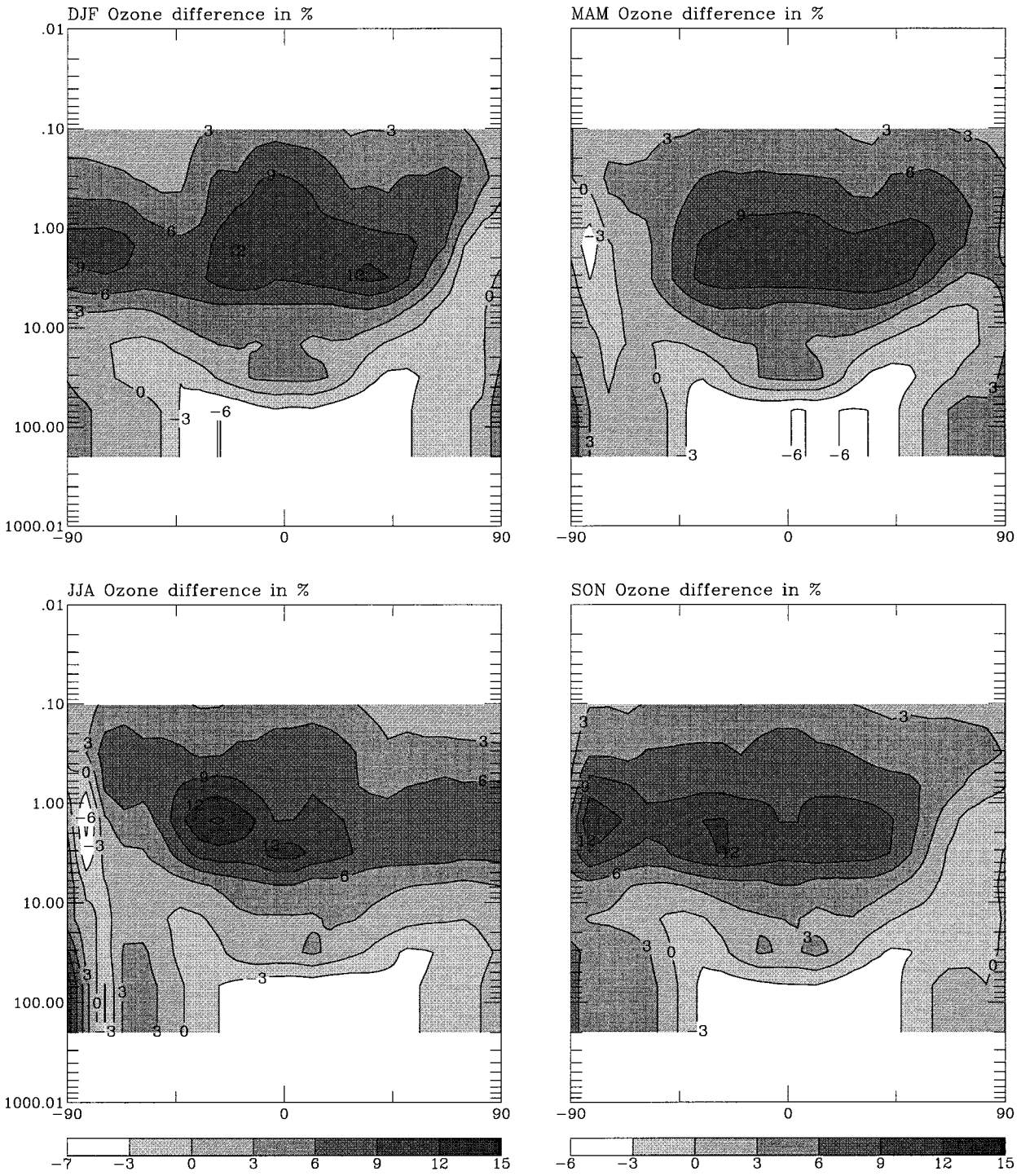

FIG. 4. Seasonal ozone change due to doubled atmospheric CO_2, including photochemical response to temperature and radiation changes. The percentage difference between zonal average ozone in the $2 \times CO_2$ and the standard CO_2 runs is shown, averaged over the last 20 yr of a 50-yr run performed for each CO_2 loading. The vertical axis is pressure in millibars, while the horizontal is latitude.

gion in the solstice seasons. The lower stratospheric temperature cools at other times, especially during March–May, leading to small ozone increases. In the southern polar region, there is also lower stratospheric cooling so that ozone increases slightly. The cooling is extremely weak from March to August, so the radiation feedback dominates even though there is little sunlight, leading to slight ozone decreases at higher altitudes.

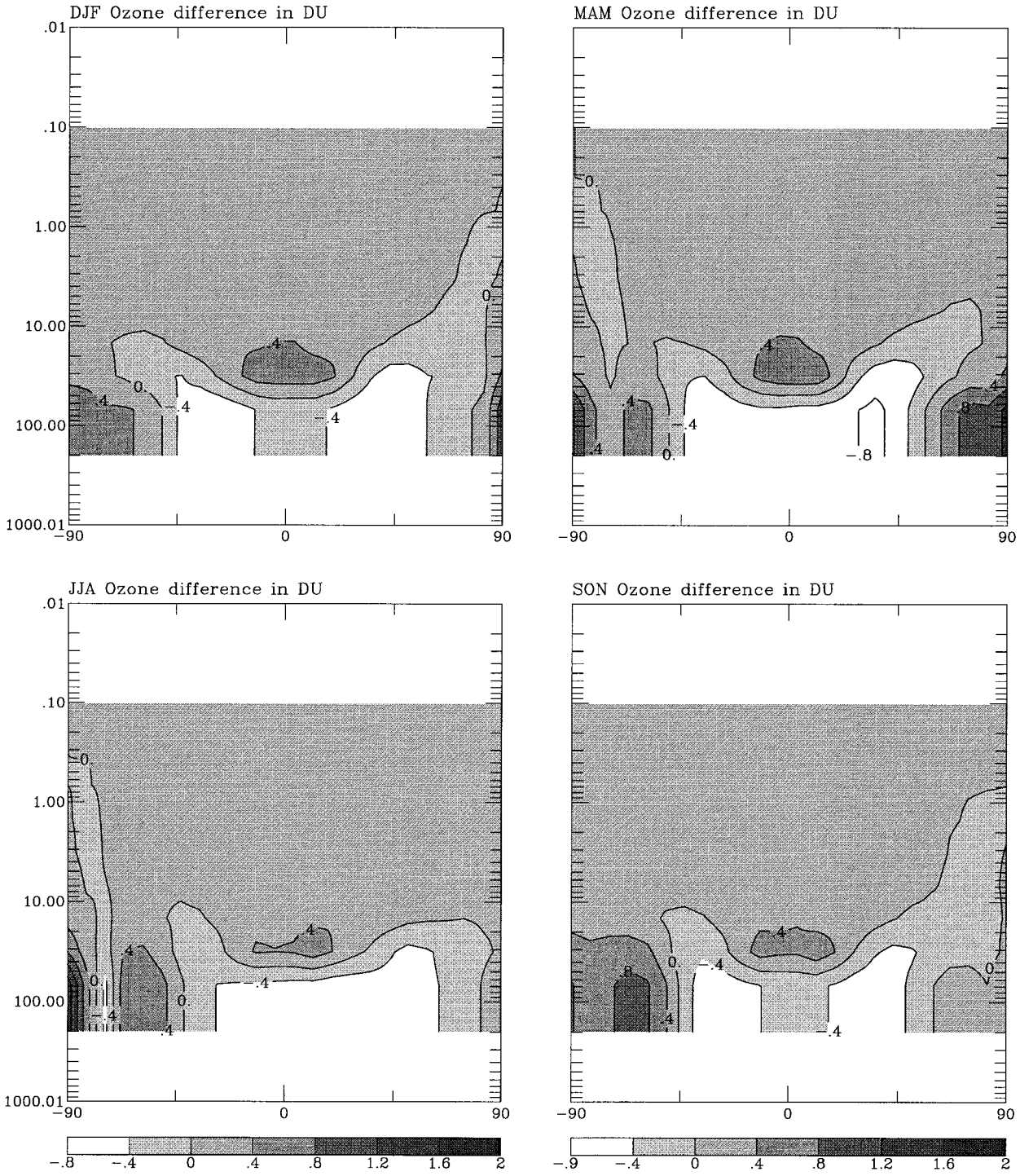

FIG. 5. Ozone change as in Fig. 4 except in DU km^{-1} atmospheric thickness.

Changes in total column ozone are shown in Fig. 6. The opposing changes in the upper and lower stratosphere combine to yield a percentage net change of much lower magnitude than the largest local changes. The large midlatitude ozone reductions in the lower stratosphere lead to net column decreases there, while the upper-stratospheric ozone increase dominates at equatorial and high latitudes, resulting in net column increases there. The high-latitude seasonal behavior follows the discussion above. Coolings in the southern

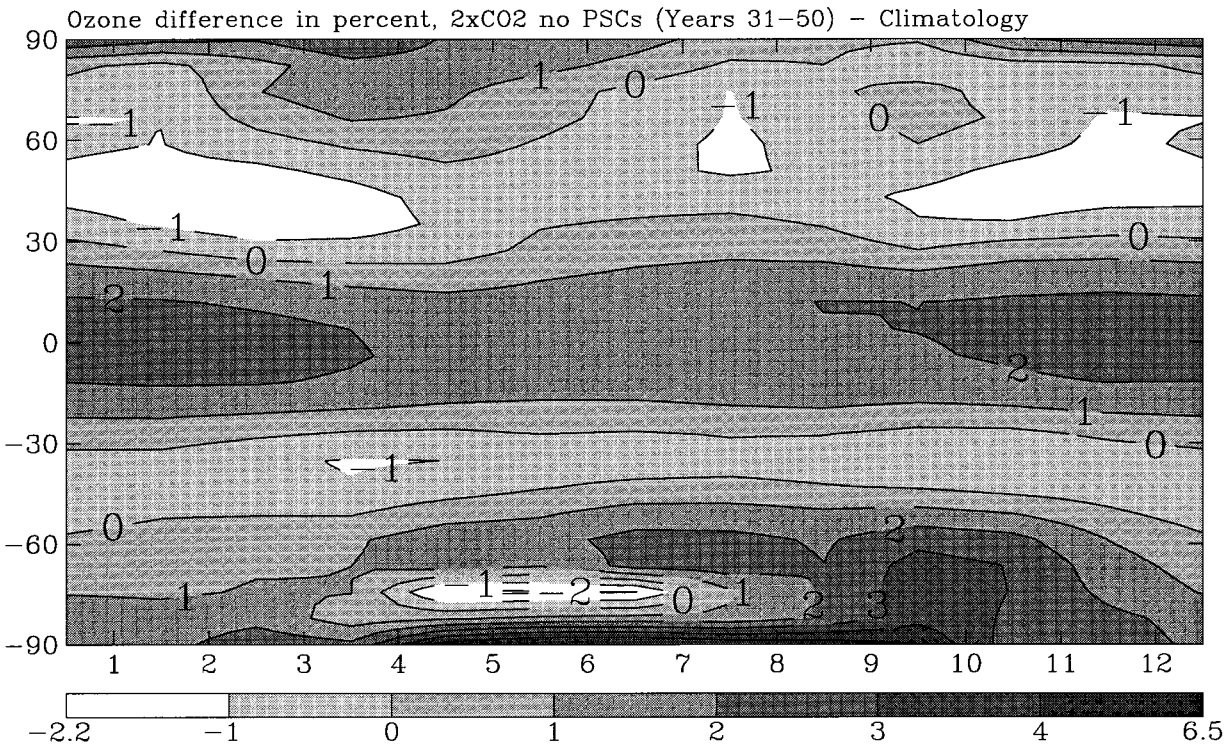

FIG. 6. Change in total column ozone due to doubling of CO_2. Data from model runs as in previous figures. The vertical axis is latitude and the horizontal is month of year.

polar region generally lead to column increases there, except during March–August, when the radiative feedback causes ozone losses. The warmings in the northern polar region that were discussed above cause column losses there. These losses extend northward from midlatitudes nearly to the pole at all times except March–May, when cooling took place in the lower stratosphere. Significant modifications induced by changed ozone transports at high latitudes will be discussed below.

The necessity of including the ozone photochemical response during the equilibration of sea surface temperatures was tested by running the model for 20 yr starting from year 25 of a $2 \times CO_2$ run without ozone feedbacks. This run was compared with the last 20 yr of the 50-yr run, which contained ozone feedbacks throughout. Years 3–10 of the new run showed large differences in the high-latitude regions when compared with the 50-yr run, with the ozone response sometimes even showing the opposite sign. Outside the polar regions, the differences were generally at the level of 1% ozone change, representing up to ~20% of the total ozone response. The agreement between the second decade of the new run and the 50-yr run was much closer, however, with all differences within the variability of the model, even in the polar regions. We therefore believe that it is not crucial to include the ozone photochemical response during sea surface temperature equilibration, though approximately a decade is required for ozone equilibration after photochemistry is included.

4. The effect of ozone photochemistry on the temperature response to $2 \times CO_2$

The effect of the ozone feedback on temperature can be seen in Fig. 7, which shows the difference in temperatures between doubled CO_2 runs with and without parameterized ozone photochemistry. Increased ozone in the upper stratosphere absorbs more radiation, leading to a warming that reduces the strength of the $2 \times CO_2$-induced cooling that occurs there by ~2°C, ~20% of the total. Exceptions are the high-latitude winters, where there is little solar radiation, so that ozone changes have minimal effect. In the middle and lower stratosphere, the percentage change of ozone is less, and so the temperature change from the inclusion of ozone photochemistry is also smaller. There is a slight cooling at equatorial and middle latitudes, with some warming at high latitudes. The temperature changes are generally less than 1°C, however, and are at the level of the model's standard deviation.

5. Comparisons with previous experiments (2D and 3D)

Ozone response to temperature changes induced by a doubling of atmospheric CO_2 has been investigated

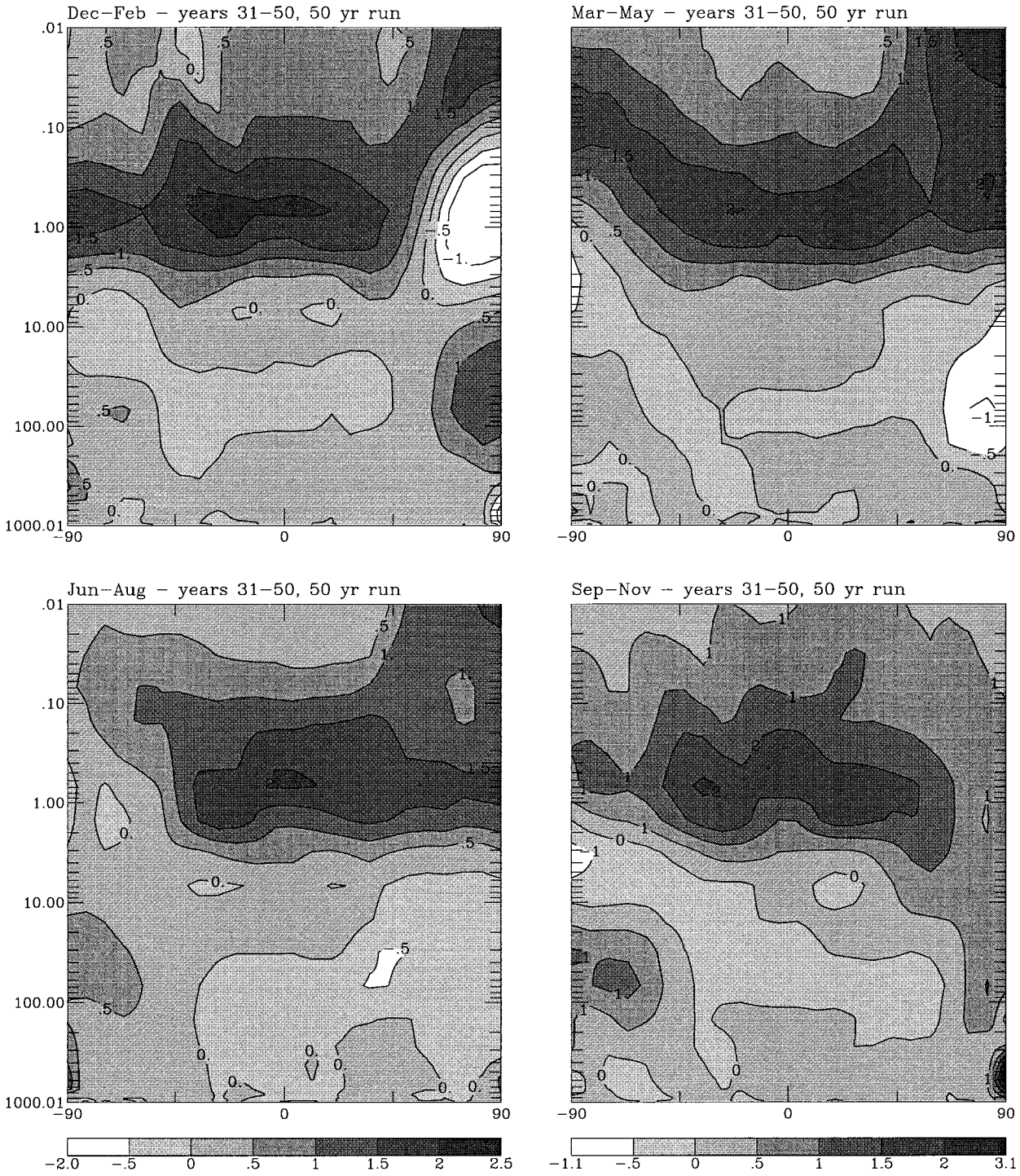

FIG. 7. Temperature change due to ozone photochemical response to 2 × CO_2. The differences between the last 20 yr of 50 yr performed with 2 × CO_2 including ozone photochemical response and 2 × CO_2 without ozone response are shown.

previously in both two-dimensional (Brasseur et al. 1990; Schneider et al. 1993) and three-dimensional models (Pitari et al. 1992; Mahfouf et al. 1994). The first three models were designed to focus on stratospheric chemistry, however, and not on long-term climate change. Though they included detailed treatments of stratospheric chemistry, rather than the parameterized approach used here, they lacked the ability to accurately simulate tropospheric dynamics or temperatures. Instead, they used prescribed tropospheric temperature

changes that were much smaller than those produced in our climate model. The fourth model, the climate model of Mahfouf et al., calculated atmospheric temperature changes based on a prescribed sea surface temperature response to $2 \times CO_2$. The SST response was calculated in the Hamburg model (Cubasch et al. 1992), which used a transient increase in CO_2. It therefore simulated the response to $2 \times CO_2$ before equilibration had taken place, so it is not surprising that they obtained an SST response that was much weaker than that found in our equilibrium–$2 \times CO_2$ experiment. This SST response in turn led to a much weaker tropospheric temperature response in the model of Mahfouf et al. than in the GISS GCM. We find that the tropospheric temperature changes, and the resulting changes in dynamics, significantly affect the ozone response to $2 \times CO_2$. In addition, the earlier studies used values of chemical reaction rate constants, which have since been revised, altering the temperature sensitivity of ozone chemistry. We now compare the temperature and ozone changes produced in our climate model with those of the other models in order to validate our parameterizations and to understand the differences.

We first discuss the differences in the temperature response to $2 \times CO_2$ between the five models. As stated previously, the three chemistry studies were done with models that used specified radiative heating rates and temperatures in the troposphere. The prescribed tropospheric temperature increase was 2°–4°C in these models in the midlatitude and equatorial upper troposphere. The climate model of Mahfouf et al. used prescribed sea surface temperature changes, giving a surface warming of only 1.4°C, compared with our warming of 5.1°C. The maximum warming in the upper troposphere in their transient experiment was less than 3°C, similar to the chemistry models and much less than the 9°–12°C maximum warming produced in the GISS GCM equilibrium experiment, as shown in Fig. 3. The impact of that large tropospheric temperature increase extends into the lower stratosphere, especially at midlatitudes. Our model shows a slight warming there, in contrast to the other models which have a slight cooling. Since the bulk of the ozone column is located in the lower stratosphere, this difference proves to be quite significant to the overall ozone response to $2 \times CO_2$.

Another important difference between the chemistry models and the one used here is the treatment of dynamical feedback from $2 \times CO_2$. The 2D model of Schneider et al. includes only radiative feedbacks from $2 \times CO_2$ and no dynamical ones. The model of Brasseur et al. does include dynamical feedbacks, but since it is also 2D, it cannot properly discern changes in wave propagation or diabatic circulation. Pitari et al. used a 3D model; however, spectral truncation and the use of a global balance approximation did not allow correct reproduction of dynamical processes in the troposphere in that model, either. The model of Mahfouf et al. also includes dynamical feedback; however, their tropospheric temperature response does not contain the large changes in the vertical and horizontal temperature gradients from a greatly warmed low-latitude upper troposphere, which are seen in the GISS GCM, so their model does not show the same increase in the residual circulation or changes in planetary wave propagation. As shown in Rind et al. (1990) and Part III, there is a marked increase in the propagation of planetary waves into the stratosphere in the $2 \times CO_2$ climate in the GISS GCM. The greater amount of eddy energy results in an increase in the intensity of the equator to pole residual circulation. The larger residual circulation increases the transport of heat to high latitudes. Thus, in the region where the percentage ozone change is largest, in the upper stratosphere around 1 mb, the GISS GCM has minima in cooling at high latitudes, about −5°C annual average, while the other models show their maximum cooling there, approximately −10° to −16°C. Ozone increases in the high-latitude upper stratosphere are therefore significantly reduced in our model compared with the earlier experiments. In addition to the dynamical influence on temperature, which affects ozone photochemistry, the altered circulation of course also affects ozone transport, as discussed below.

As discussed in the previous paragraphs, the greatest differences in the temperature response to $2 \times CO_2$ between our results and the results of the other models are at middle and high latitudes. We obtain stratospheric temperature changes that are fairly similar in the equatorial region, and we will therefore compare the ozone response in that region first. Between 15°N and 15°S, the other models find ozone column changes of 2–4 DU (Brasseur et al. 1990), 0–10 DU (Pitari et al. 1992), 4–6 DU (Schneider et al. 1993), and approximately 0–7 DU (Mahfouf et al. 1994), while we find a column increase of 3–8 DU in our GCM. Our values therefore agree quite well, though the range of results is large. Comparison of the vertical profiles of ozone change are a better test, but results were only presented from the Brasseur et al. and Schneider et al. models. In the equatorial upper stratosphere, where transport is not important, Brasseur et al. find a maximum increase in ozone abundance of ~20% at 1–2 mb in June, where their temperature decrease is −8° to −9°C. Our maximum increase is only about 14% at 2–4 mb in June, for a temperature decrease of −8° to −10°C. We attribute this difference to the influence of the updated chemical reaction rate constants used in the derivation of our chemistry parameterizations. The JPL 1985 reaction rates used by Brasseur et al. were significantly different from the current rates. Most importantly, the activation energies of the reactions $O + O_3 \rightarrow 2O_2$, $O_3 + HO_2 \rightarrow OH + 2O_2$, $O + NO_2 \rightarrow NO + O_2$, and $O + ClO \rightarrow Cl + O_2$ were all larger, resulting in an increased temperature sensitivity relative to the current reaction rate constants. This is reflected in the larger ozone increase calculated in the older model for a similar temperature decrease. When we use the old reaction rate

constants in our 1D model, we derive a similar sensitivity to that exhibited in the Brasseur et al. results. Schneider et al. find a maximum ozone increase of ~15% in the equatorial upper stratosphere at ~1.5–3 mb in December, for a temperature decrease of −10 K. In December, our model produces a temperature decrease of −7 to −8 K, which leads to an ozone increase of ~11%, equal in sensitivity to that of Schneider et al. Thus, we obtain good agreement with the available vertical profiles of ozone change from the chemistry models. The overall agreement between our results and the results of the stratosphere chemistry models in the equatorial regions gives credence to the chemistry parameterizations we have used.

At middle latitudes, the ozone column in our GCM decreased by 0%–2%. This result is very different from the other models, which found column increases of +2%–5% (Schneider et al. 1993), +0%–2% (Brasseur et al. 1990), +4%–8% (Pitari et al. 1992), and +2%–10% (Mahfouf et al. 1994). The other models did not find the large ozone reductions in the lower stratosphere that we found, since they didn't have a large tropospheric warming. At high latitudes, the results from the five models diverge more strongly. Brasseur et al. and Pitari et al. found ozone column increases of −1% to +3% and −1% to +7%, respectively, similar to our −2% to +5% results. The seasonal variation also matches quite well with these two models. Both show a slight column loss at high southern latitudes during the austral fall–winter and column increase before and after in agreement with our results shown in Fig. 6. Schneider et al. and Mahfouf et al. found column increases of +6%–9% and +4%–9%, respectively, at high southern latitudes, however, with increases at all times of the year in both models. The reason for their larger values and lack of the seasonal variation seen in the other models is not clear but is perhaps related to differences in or the lack of the $2 \times CO_2$ feedback on the residual circulation, which strongly influences the high-latitude temperature response. The model of Mahfouf et al. also found large increases in the winter high-latitude ozone column in the Northern Hemisphere, which they attribute to increased poleward and downward transport of ozone. When ozone transport is included in our model, we do see larger wintertime high-latitude column increases than with chemistry only, as discussed below, but still not up to the levels seen in the Météo-France model.

6. Ozone response to $2 \times CO_2$ including heterogeneous chemistry on PSCs

A physically realistic parameterization of the heterogeneous chemistry responsible for polar ozone depletion was included directly into the GCM. In this parameterization, we calculate the fraction of available chlorine activated into chlorine monoxide (ClO) at each point, based upon the modeling of Shindell and de Zafra (1996, 1997). The calculations included gas-phase chemistry and heterogeneous reactions on Type I (nitric acid trihydrate) and Type II (water ice) polar stratospheric clouds PSCs and on STS surfaces. Over time, particles were removed from the atmosphere through gravitational settling or by evaporation when temperatures warmed. Once activation had taken place and sunlight was present, active chlorine was partitioned between ClO and the ClO dimer as a function of sunlight and temperature based on photochemistry, as in Shindell and de Zafra (1996).

In the GCM experiments, recent measurements of atmospheric chlorine loading were used to set the total available amount (von Clarmann et al. 1995; Woodbridge et al. 1995). Any time that temperatures are cold enough for PSCs to form, full activation is assumed to take place in 5 h (though ozone depletion also requires sunlight to continuously convert active Cl into ClO). Deactivation is a function of elapsed sunlit time since the last exposure to PSCs. When sunlight is present, photochemical reactions that create short-lived free radicals such as OH and NO_2 are initiated. These radicals then convert chlorine species from active forms back into reservoirs. Active chlorine abundance decreases linearly to zero in 80 sunlit hours in the GCM, following the deactivation rate seen in the one-dimensional modeling. This photochemical deactivation rate is rapid compared to transport times in the lower stratosphere, so that transport is not overly important for chlorine deactivation rates (though it could influence the relative rate at which chlorine reservoirs are reformed). Ozone depletion depends on the square of the chlorine monoxide abundance, from the rate limiting ClO dimer formation reaction of the catalytic ozone loss cycle, $ClO + ClO + M \rightarrow Cl_2O_2 + M$, so that the neglect of nonlinearities in the chlorine deactivation rate at low ClO amounts that were seen in the one-dimensional modeling should be insignificant.

Ozone depletion takes place at each point in the GCM where there is both active chlorine and sunlight is available to convert the active chlorine into ClO. Ozone loss is calculated according to $d(O_3)/dt = -2k(ClO)^2(M)$, where (ClO) is the concentration of chlorine monoxide, k is the rate constant of the ClO dimer formation reaction given above, and (M) is the concentration of background gas molecules. An additional contribution of ~15% from bromine chemistry is also included. Ozone recovery is parameterized so that ozone losses are restored based on the photochemical lifetime of ozone at each altitude, as calculated in the 1D-model.

In both the $2 \times CO_2$ and control runs containing chemistry on PSCs, the amount of mountain wave drag in the GCM was reduced to one-quarter of its previous value to allow a more realistic simulation of temperatures in the Southern Hemisphere polar lower stratosphere, which were otherwise too warm. For equilibration, both runs were continued with the reduced drag coefficient for 10 yr after the 50 yr already run. Five

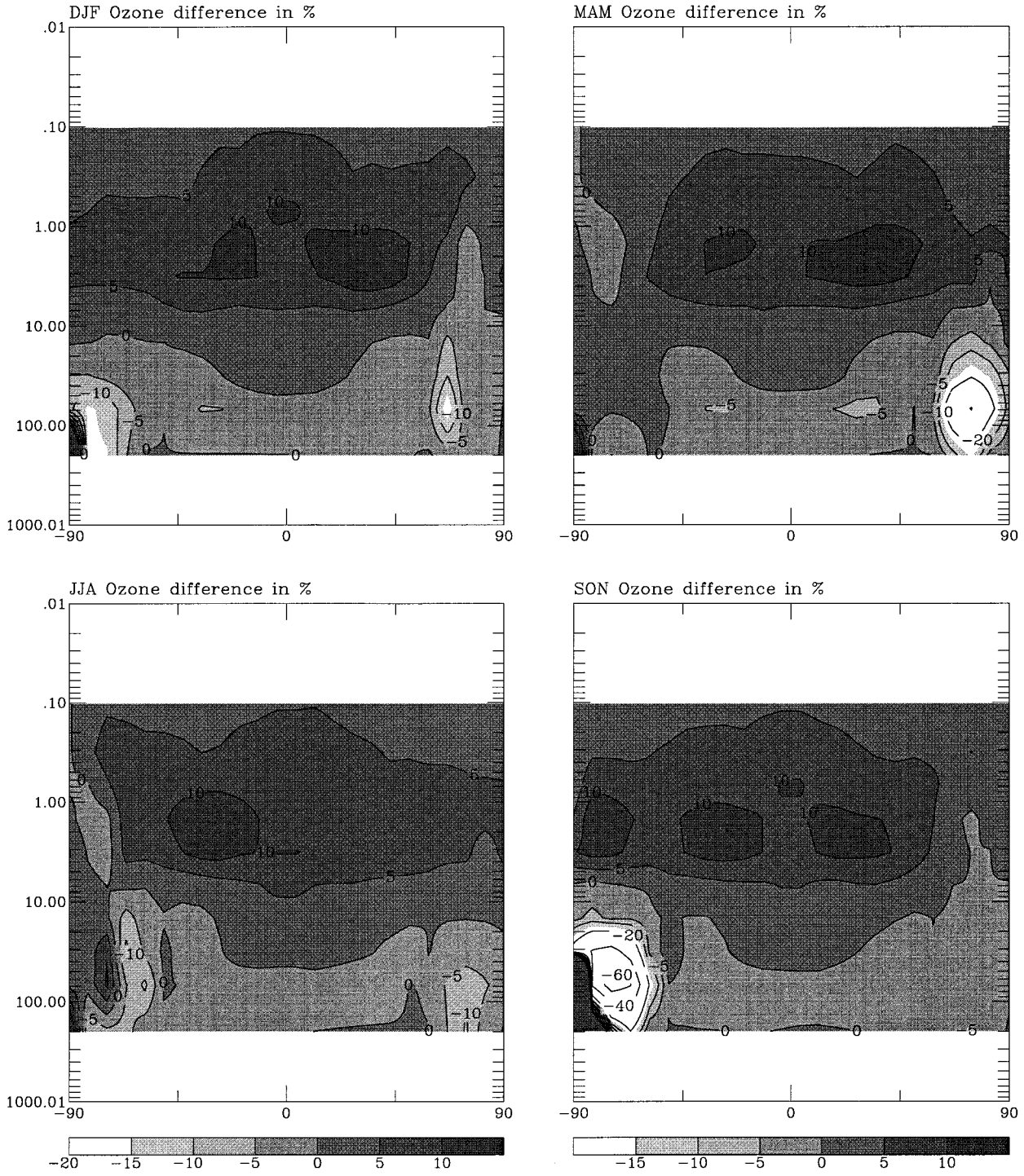

FIG. 8. Seasonal ozone change as in Fig. 4 but for 2 × CO_2 and control runs that both included chemistry on PSCs.

(2 × CO_2) and six (1 × CO_2)-year runs were then performed including the parameterized chemistry on PSCs.

The percentage ozone changes due to 2 × CO_2 from the model run with parameterized ozone chemistry including heterogeneous chemistry are given in Fig. 8. We show the difference between the doubled CO_2 run and the 1 × CO_2 simulation, which also included parameterized heterogeneous chemistry. The general pattern of increases in the upper stratosphere and decreases in the equatorial and midlatitude lower stratosphere is quite similar to that shown in Fig. 4 for the run without

PSC–STS chemistry. Given that the lower stratosphere cools at high latitudes in the doubled CO_2 atmosphere, we would expect an increase in the abundance of particle surfaces, leading to greater winter–spring ozone loss. Indeed, there is significantly less ozone in the high-latitude lower stratosphere of both hemispheres during the polar winter and spring. The percentages can be misleading, however. Since most of the ozone was already destroyed in the southern spring lower stratosphere, percentage changes are differences between small amounts of remaining ozone. For example, the large percentage increase of ozone near the South Pole in September–November in Fig. 8 actually represents only a few DU less ozone destruction out of a large total loss. We show the same ozone changes in DU in Fig. 9. The main effects are obviously the significant increases in polar lower stratospheric ozone losses, especially in the northern spring.

To further examine the changes in polar lower stratospheric ozone losses, we show the percentage ozone losses in April and October for the $1 \times CO_2$ and $2 \times CO_2$ cases individually in Fig. 10. Antarctic spring ozone losses extend to higher altitudes and to lower latitudes in the $2 \times CO_2$ atmosphere. Maximum column losses increase by ~30 DU due to the extra depletion at higher altitudes, while the area in which there has been 50% or greater column ozone loss increases by ~40%. In the Northern Hemisphere, interannual and spatial variability is much greater. In the $1 \times CO_2$ atmosphere, maximum local losses of up to 54% occurred in years with cold temperatures and subsequent sizable ozone losses. However, local zonal mean ozone loss averaged over a 6-yr run was 8% at most. In the $2 \times CO_2$ case, we find a large decrease in the frequency of sudden warmings in the northern winter, as the westerly zonal winds are enhanced, limiting the ability of wave two to propagate into the stratosphere, as discussed in Part III. Though there is a general increase in transport of heat to high latitudes by the diabatic circulation, as wave one is amplified in the $2 \times CO_2$ case leading to slight warming, it is more than compensated for by the lack of sudden warmings in most years.

In years without sudden warmings, there is greatly increased ozone loss in our model, in agreement with the results of Austin and Butchart (1994). The GISS GCM reproduces observed variability fairly well, though it does slightly underestimate wave amplitude variability, as shown in Rind et al. (1988b). Though the interannual variability in the northern spring is reduced in the $2 \times CO_2$ run, as there are fewer sudden stratospheric warmings, it remains large. During the 5 yr of the model run, maximum local zonal mean springtime ozone losses ranged from 10% to 88%. Despite the significant variability, the $2 \times CO_2$ influence is clear, with the local zonal mean ozone loss averaged over the 5-yr run giving values as high as 55%, as compared with the ~12% seen in the $1 \times CO_2$ case. Furthermore, large ozone holes formed in three out of the five model years. Note again that these results do not include the transport of depleted ozone (discussed below) and that current chlorine levels have been used. Total column ozone losses are shown in Fig. 11. The ozone hole in the Southern Hemisphere is larger, more severe, and lasts for a significantly longer period. The average ozone hole formed in the Arctic is ~45% the strength of the average $1 \times CO_2$ Antarctic hole. The variability is large in the Arctic though, with ozone losses ranging from ~15% to ~75% of those typically seen in the Antarctic.

The temperature changes due to $2 \times CO_2$ with ozone chemistry including PSCs are shown in Fig. 12. Equatorial and middle latitudes show a temperature response quite similar to that in the run without PSCs shown in Fig. 3. There is an average cooling in the Arctic lower stratosphere in winter due to reduced frequency of sudden warmings and resulting ozone losses and a very large cooling in spring resulting from the Arctic ozone hole. The Arctic springtime upper stratosphere also shows considerable ozone-hole-induced warmings not seen in the run without PSCs (see Fig. 3). Changes also take place in the stratosphere over the Antarctic. The cooling in the lower and middle stratosphere during September–November increases with the ozone loss in the $2 \times CO_2$ atmosphere. Additionally, the longer duration of the Antarctic ozone hole leads to a significant cooling in the lower stratosphere during December–February. Warmings at high altitude in the austral spring and summer are also significantly larger. The changes at high latitudes due to the formation/enhancement of an ozone hole agree quite well with the temperature response to an ozone hole in a $1 \times CO_2$ atmosphere found in our model (Shindell et al. 1997) and in other models (Kiehl et al. 1988; Cariolle et al. 1990; Mahlman et al. 1994). These models all showed lower stratospheric coolings due to decreased radiative absorption accompanied by upper-stratospheric warmings due to dynamical heating.

Pitari et al. (1992) also investigated the ozone response to $2 \times CO_2$ including heterogeneous chemistry on PSCs in their experiment. They found an increase in ozone destruction of 10–40 DU in the Antarctic spring, in good agreement with our results. In the Northern Hemisphere, they found only a 10-DU increase in column ozone loss. In their model, a fairly warm year was simulated, and ozone transport from midlatitudes tended to balance polar losses. In contrast, Austin et al. (1992) found large ozone losses in the Arctic in a $2 \times CO_2$ atmosphere during a cold year, similar in magnitude to our results. Clearly, the amount of ozone loss is strongly influenced by the frequency of sudden warmings that create ''warm'' years. We note that the radiative influence of PSCs was not included here, though this effect is thought to be fairly insignificant (Rosenfield 1993).

7. Changes in ozone transport

It was not possible to include changes in the transport of ozone interactively in our experiment. Instead, they

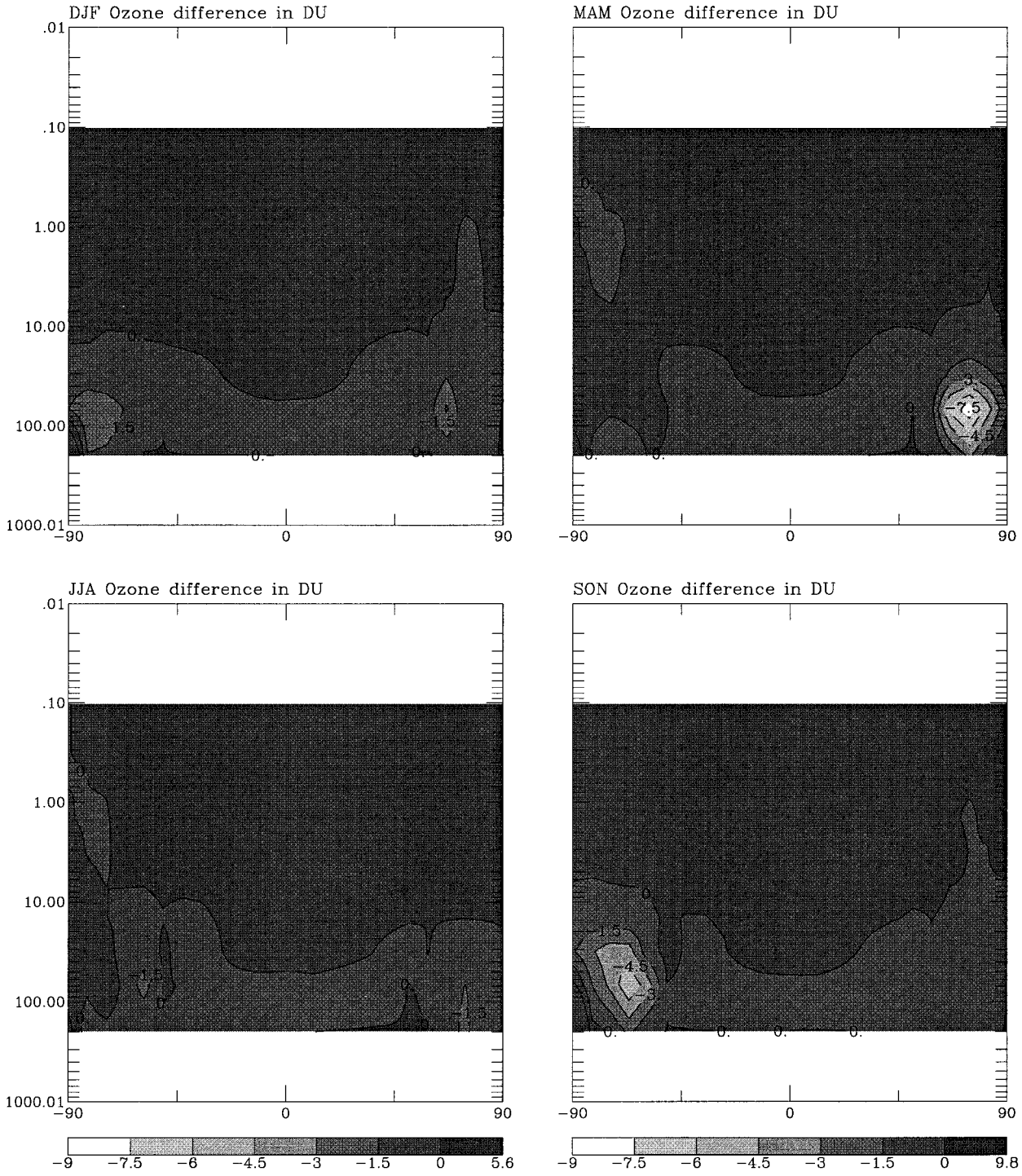

FIG. 9. Ozone change as in Fig. 8 except in DU km^{-1} atmospheric thickness.

have been calculated off-line as the product of the horizontal and vertical transports and the ozone gradients in each direction, which gives the transport flux in and out of each grid box. For the transport terms, the transformed Eulerian circulation (V^*) was used for the horizontal motion, and the divergence of this circulation for the vertical motion (W^*), so that to the extent that this circulation is driven by diabatic heating and Eliassen–Palm flux divergence, it includes both mean- and eddy-forcing effects. The sum of the fluxes gives the net ozone convergence or divergence for each individual grid box. Average ozone convergences were calculated

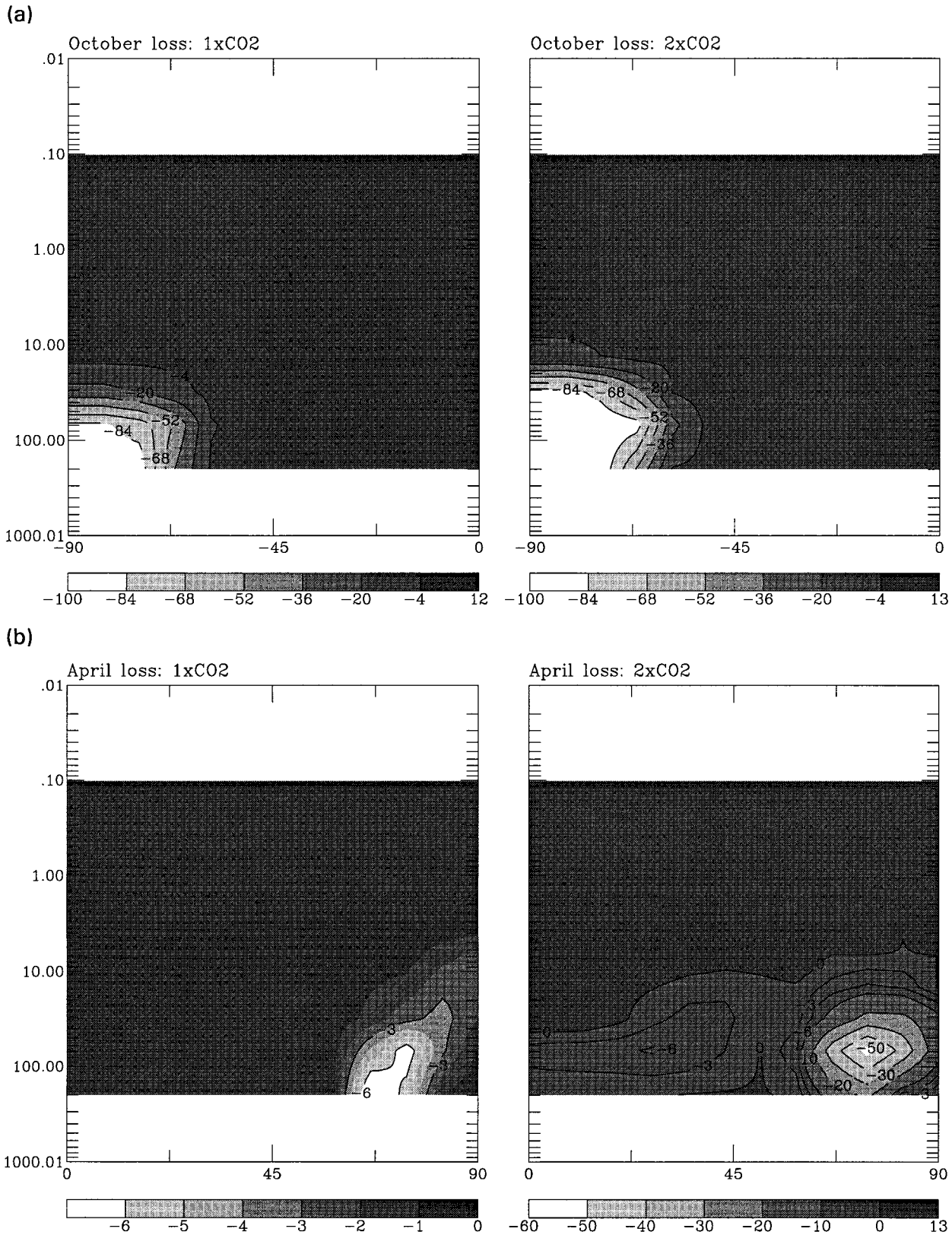

FIG. 10. Percentage ozone changes in the 1 × CO_2 and 2 × CO_2 cases including chemistry on PSCs. Results are given for months with severe ozone depletion: October in the Southern Hemisphere and April in the Northern Hemisphere. Note change in scales between plots.

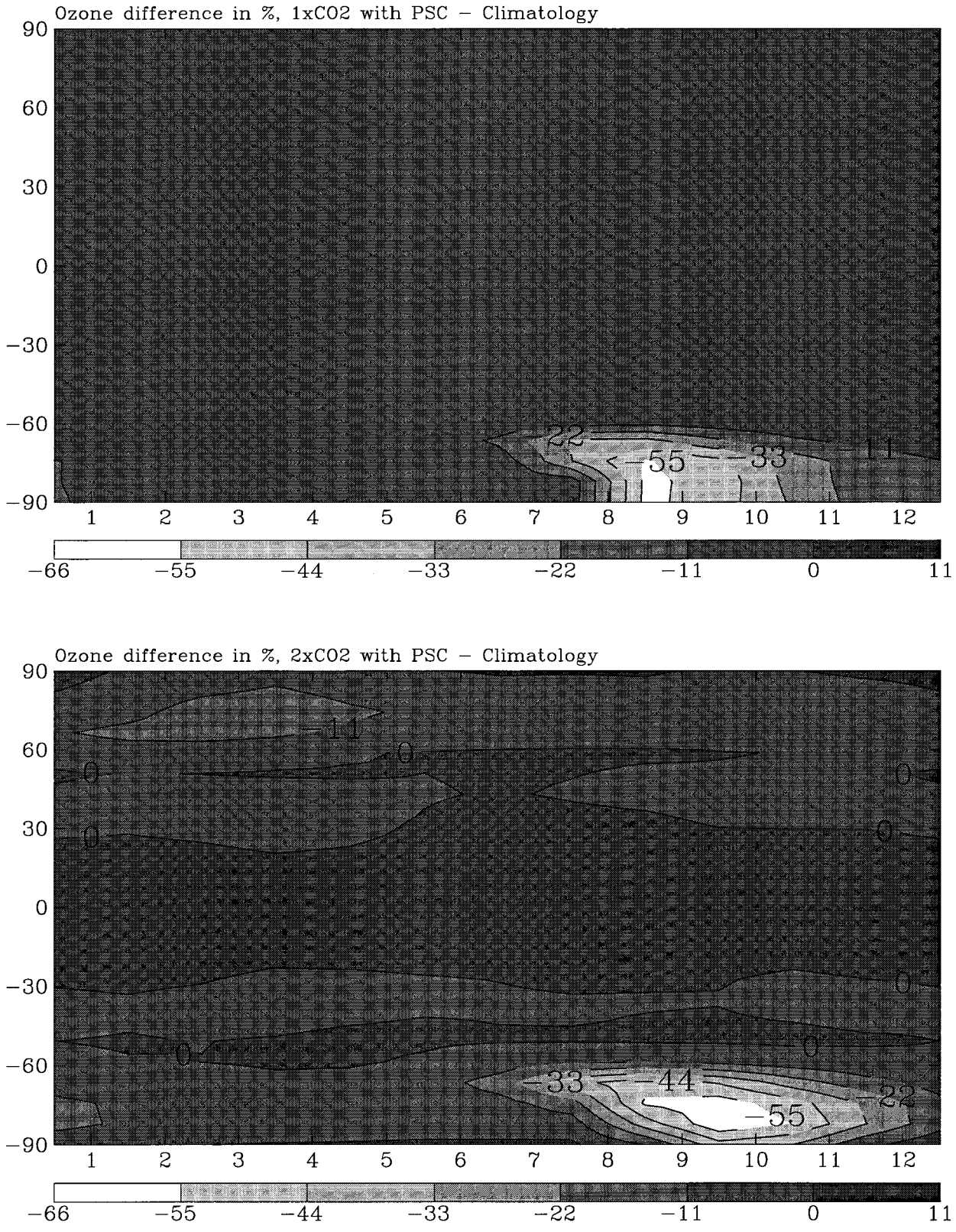

FIG. 11. Column ozone changes in the 1 × CO_2 and 2 × CO_2 cases including chemistry on PSCs. The vertical axis is latitude and the horizontal is month of year.

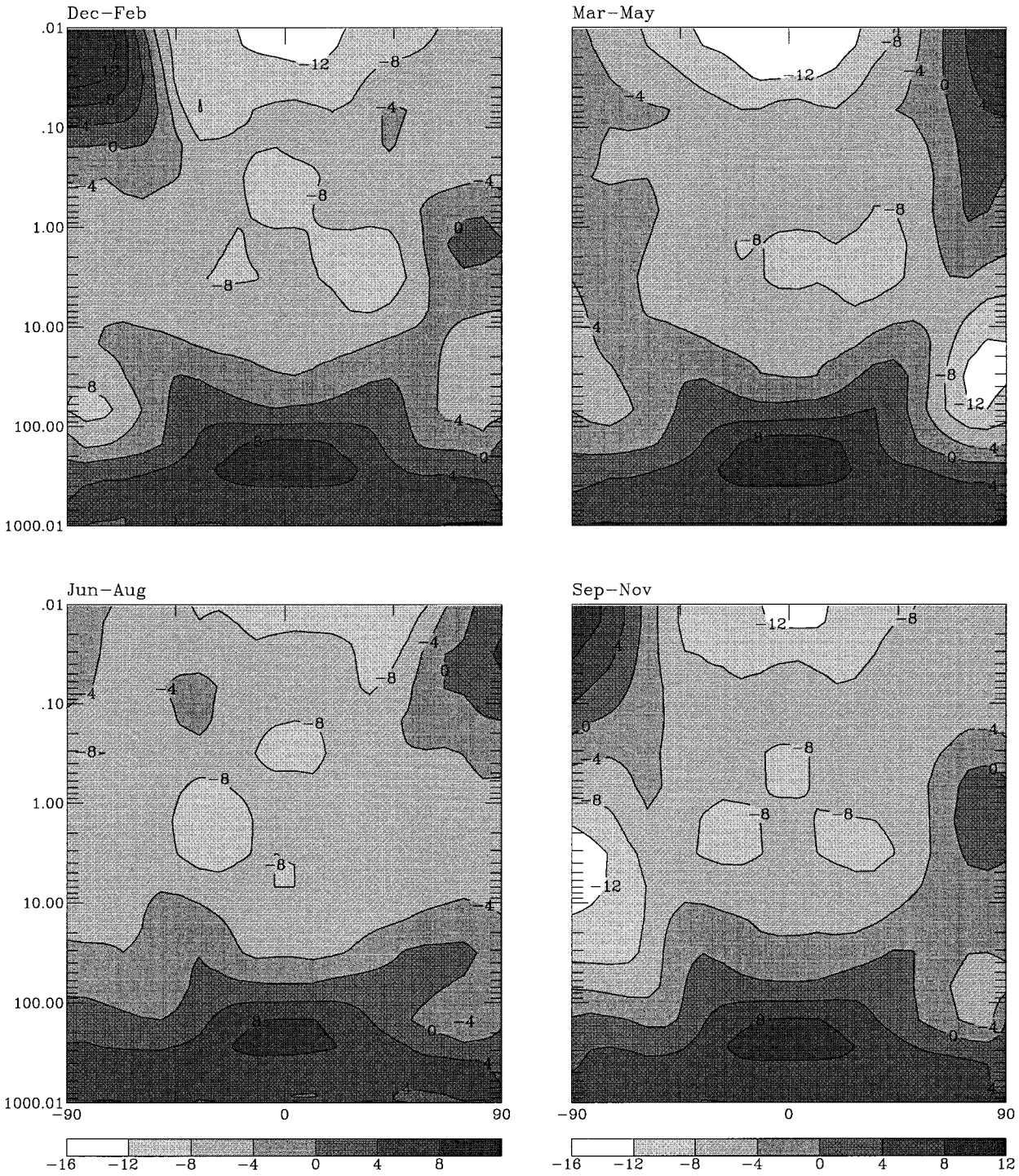

FIG. 12. Temperature changes as in Fig. 3 but for 2 × CO_2 and control runs that included chemistry on PSCs.

for the 5-yr 2 × CO_2 run including heterogeneous chemistry on PSCs and compared with the averages from the 6-yr control run, which also included PSC chemistry.

Figure 13 shows the circulation changes between the 2 × CO_2 run and the control run (1 × CO_2) for vertical and horizontal motion during the solstice seasons. During both seasons, the increased tropical temperatures enhance the rising motion (negative values) due to latent heat release associated with the intertropical convergence zone (ITCZ). In the Northern Hemisphere winter, the model splits the ITCZ into two branches, so we see two sets of rising columns with subsidence in between.

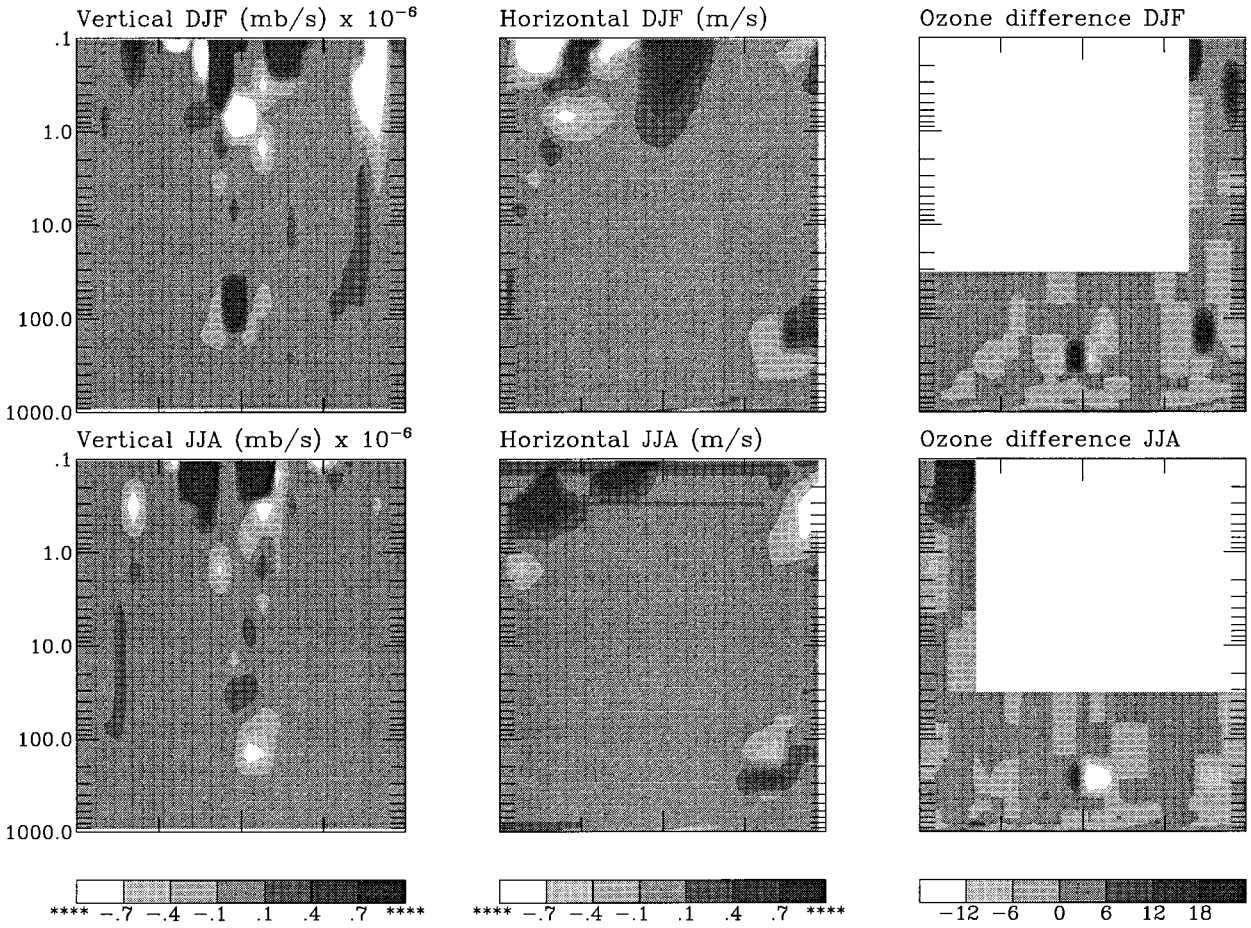

FIG. 13. Changes in circulation between 2 × CO_2 and control runs. Transformed Eulerian circulation was used for the horizontal motion and the divergence of this circulation for the vertical motion. A positive value is up or north for vertical and horizontal motions, respectively. Also shown is the resulting seasonal percent change in ozone calculated from the altered transport convergences.

During June–August, the ITCZ is correctly located just north of the equator, where a strong upwelling is shown. In both seasons, there is an enhancement of the descent rate in the middle stratosphere at high latitudes in the darkness of the polar night. The horizontal transports show their largest differences in the lower stratosphere, where the more stable polar vortex that forms in the 2 × CO_2 run blocks the mean meridional flow, reducing the northward transport at the vortex boundary around 65°N.

We use V^* and W^* multiplied by the ozone gradient to calculate the ozone convergence at each point, which is then allowed to change the ozone gradient. The results are applied only to the areas where transport dominates over photochemistry, that is, below about 30 mb in sunlit regions and at all altitudes during the polar night (Perliski et al. 1989). The calculation has been iterated for 3 months, with a time step of 100 min, to get the seasonal transported ozone changes between the 2 × CO_2 run and the control run. This is an appropriate duration given that the transports vary on a seasonal timescale, and the photochemical lifetime of ozone is fairly long below 30 mb and during polar night. The resulting percentage changes in ozone are also shown in Fig. 13. In December–February, there is a large buildup of ozone in the lower stratosphere just outside the polar vortex, resulting from the reduction in transport across the enhanced vortex wall found in the 2 × CO_2 run. Additionally, there is an increase in ozone in the Arctic upper stratosphere in the polar darkness. If only Eulerian mean motions are considered, the increased descent in this region leads to ozone decreases; the calculated increase results from increased convergence of northward eddy energy in the middle stratosphere, which forces rising motion around 60°N. This motion carries ozone-rich air into the upper stratosphere, where it combines with an increased ozone flux from above due to descent to cause a large net ozone convergence around 0.3 mb. Similar rising motions in the middle stratosphere and increased transport into the upper stratosphere are seen in the southern polar night. Near the equator, the largest changes in ozone are seen near the tropopause. Upwelling leads to ozone reduction, while descent leads to ozone increases. In general, the changes

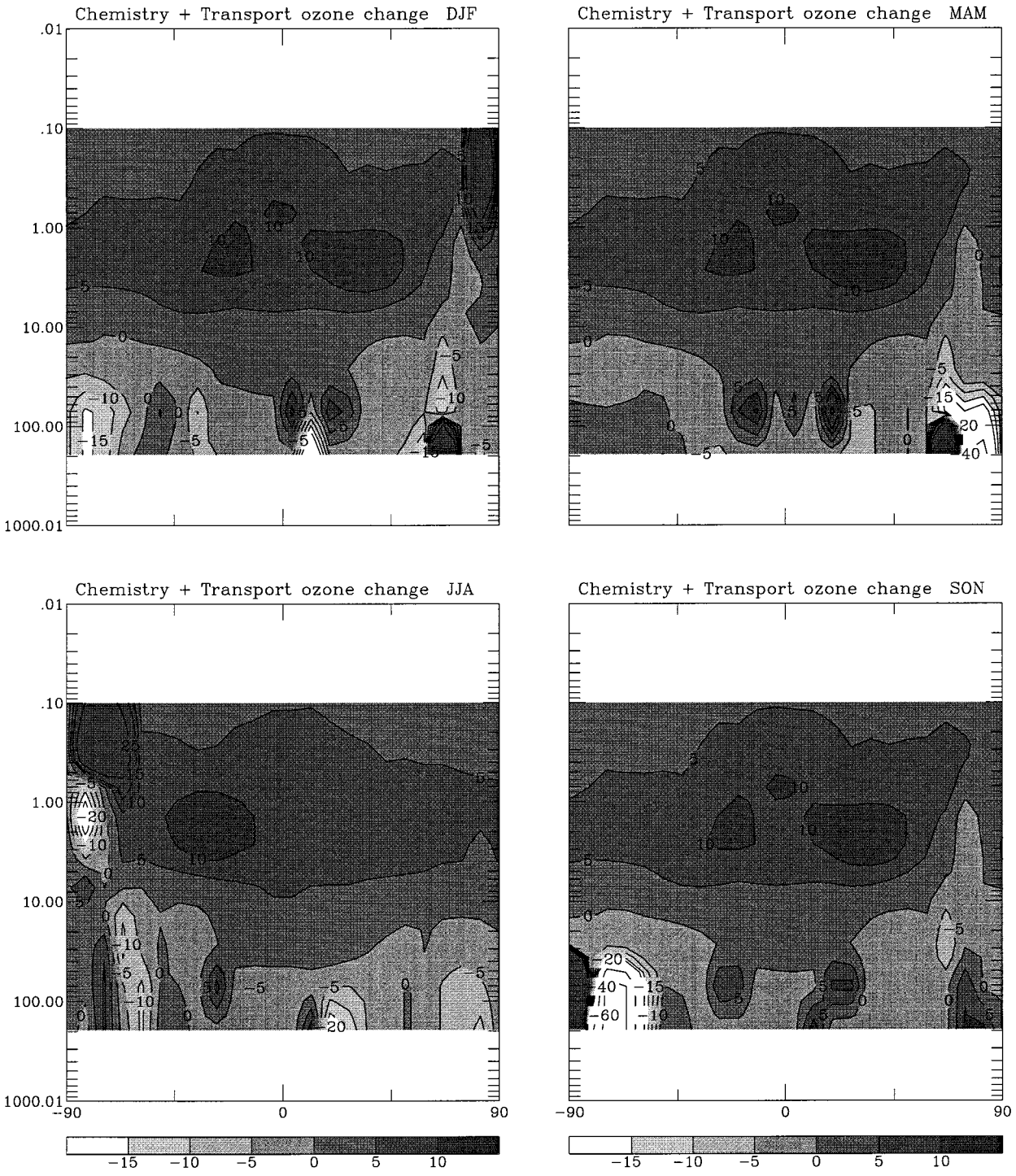

FIG. 14. Seasonal ozone change difference between the 2 × CO_2 and control runs as in Fig. 8 but for the sum of on-line chemistry and off-line transport changes.

at middle and low latitudes are fairly small, mostly falling within the 6% contour.

In Fig. 14, we show the net seasonal ozone change from chemistry plus transport, assuming that the chemistry and transport changes are additive. In the lower stratosphere and the polar winter upper stratosphere, the ozone changes due to transport are similar in magnitude to or even larger than the chemically induced changes, as can be seen by comparing with the ozone change due to chemistry alone shown in Fig. 8. In the polar dark-

ness, especially in the southern vortex, the ozone divergence in the middle stratosphere combines with the residual chemical depletion in that region to create a large net reduction in ozone amounts around 0.8–4.5 mb, with increases predominantly driven by transport above and below those altitudes. In both hemispheres, the enhanced descent within the polar vortex brings an influx of ozone down into the lower stratosphere, reducing the heterogeneous chemical depletion at the upper levels of the ozone hole. Furthermore, in the Northern Hemisphere, the blocking of meridional transport set up by the stronger polar vortex that forms in the 2 $\times$ CO_2 run leads to a buildup of ozone at latitudes near the edge of the vortex. During June–August, after the vortex breaks up, transport of ozone washes out the differences between the region of severely depleted ozone and the region of the ozone buildup. In the equatorial and middle latitude lower stratosphere, ozone changes due to transport result in net increases in ozone amounts in several locations, while chemistry alone led to ozone losses everywhere. Transport reductions in ozone combine with chemical reductions only in the solstice seasons at northern low latitudes, where increased upwelling in the ITCZ leads to large ozone decreases near the tropopause.

In a further experiment, the new ozone field resulting from chemistry and transport changes induced by CO_2 doubling was put back into the GCM to assess the impacts on temperatures and dynamics. In the polar darkness, the new ozone resulted in minor changes in temperatures due to the modified absorption of longwave radiation ($\sim$2 K). Perhaps the most significant impact is in the Arctic lower stratosphere, where the decreased transport of ozone into the polar vortex leads to less absorption there, so that the temperatures within the vortex become slightly cooler ($\sim$1 K), which could result in even greater ozone losses. Temperature changes of up to 3° were found at middle and equatorial latitudes in the lower stratosphere, but for small local areas only. Dynamics were relatively unaffected by the altered ozone.

Total ozone column amounts are shown in Fig. 15. The two panels show identical results with two different scales, so that the top panel highlights the severe polar springtime ozone losses, while the lower panel shows the lower latitude response more clearly. We focus first on the polar regions. Comparing the chemistry plus transport-2 $\times$ CO_2-induced ozone column changes (top panel) to the chemistry-only column changes (lower panel of Fig. 11), we see that the addition of the ozone transport response to 2 $\times$ CO_2 has had the most significant effects at high northern latitudes. As discussed above, the enhanced northern polar vortex has blocked the northward transport of ozone near the vortex edge with respect to the control 1 $\times$ CO_2 run, leading to an ozone buildup around 60°–70°N, and decreased ozone abundances within the vortex. The combination of chemistry and transport now leads to Arctic ozone losses of up to 30% of the total column (roughly half those of the Antarctic), though of limited geographical extent. Additionally, during the polar darkness of October–December, the increased circulation leads to an overall increase in the high-latitude ozone column.

At middle and equatorial latitudes (bottom panel), the inclusion of ozone transports has had a very large impact on the 2 $\times$ CO_2-induced ozone column changes compared with chemistry alone (Fig. 6, which does not include PSCs). Ozone transport changes have led to larger increases in the equatorial ozone column, roughly doubled the column decreases at northern midlatitudes, and reduced the area at southern midlatitudes that shows column decreases.

8. Surface UV flux and temperature changes

Ozone changes directly affect the habitability of the earth through their impact on UV radiation reaching the earth and on surface temperatures. The influence of 2 $\times$ CO_2-induced ozone changes can be assessed by comparison of fluxes and temperatures when ozone chemical and transport responses are included in the 2 $\times$ CO_2 case relative to 2 $\times$ CO_2 without ozone response. The photochemical ozone changes cause the UV radiation incident at the surface to increase slightly in the Northern Hemisphere ($+0.11$ W m^{-2}), and decrease in the Southern (-0.14 W m^{-2}). Globally averaged, however, the mean surface temperature increases by $\sim$5.1°C versus 1 $\times$ CO_2, either with or without ozone chemical response to 2 $\times$ CO_2. This value is also only minimally affected by the inclusion of chemistry on PSCs. Thus, the ozone changes primarily affect temperatures in the stratosphere on a global scale (see Fig. 7) and have little effect on global mean surface temperatures.

Ozone response to 2 $\times$ CO_2 does impact surface temperature on a regional scale, however. As shown in Figs. 6 and 15, significant reductions in column ozone due to 2 $\times$ CO_2 occurred at northern midlatitudes. In this region, where a large portion of the world's population lives, the ozone losses lead to larger changes in UV and temperature. From 31° to 55°N, there was a mean increase in surface UV radiation of $+0.8$ W m^{-2} due to the chemical ozone loss alone. With the inclusion of ozone transport, the increase was $+1.3$ W m^{-2}. These are increases of $\sim$6% and $\sim$10% in the UV radiation reaching the surface at these latitudes, respectively. The surface temperature in this band increased by $\sim$0.3°C relative to the 2 $\times$ CO_2 case without ozone response in both cases. These midlatitude results were quite similar with or without PSCs.

9. Summary

We have parameterized the photochemical response of ozone to temperature to calculate the ozone changes induced by a doubling of atmospheric carbon dioxide. The additional feedback of ozone change causing dif-

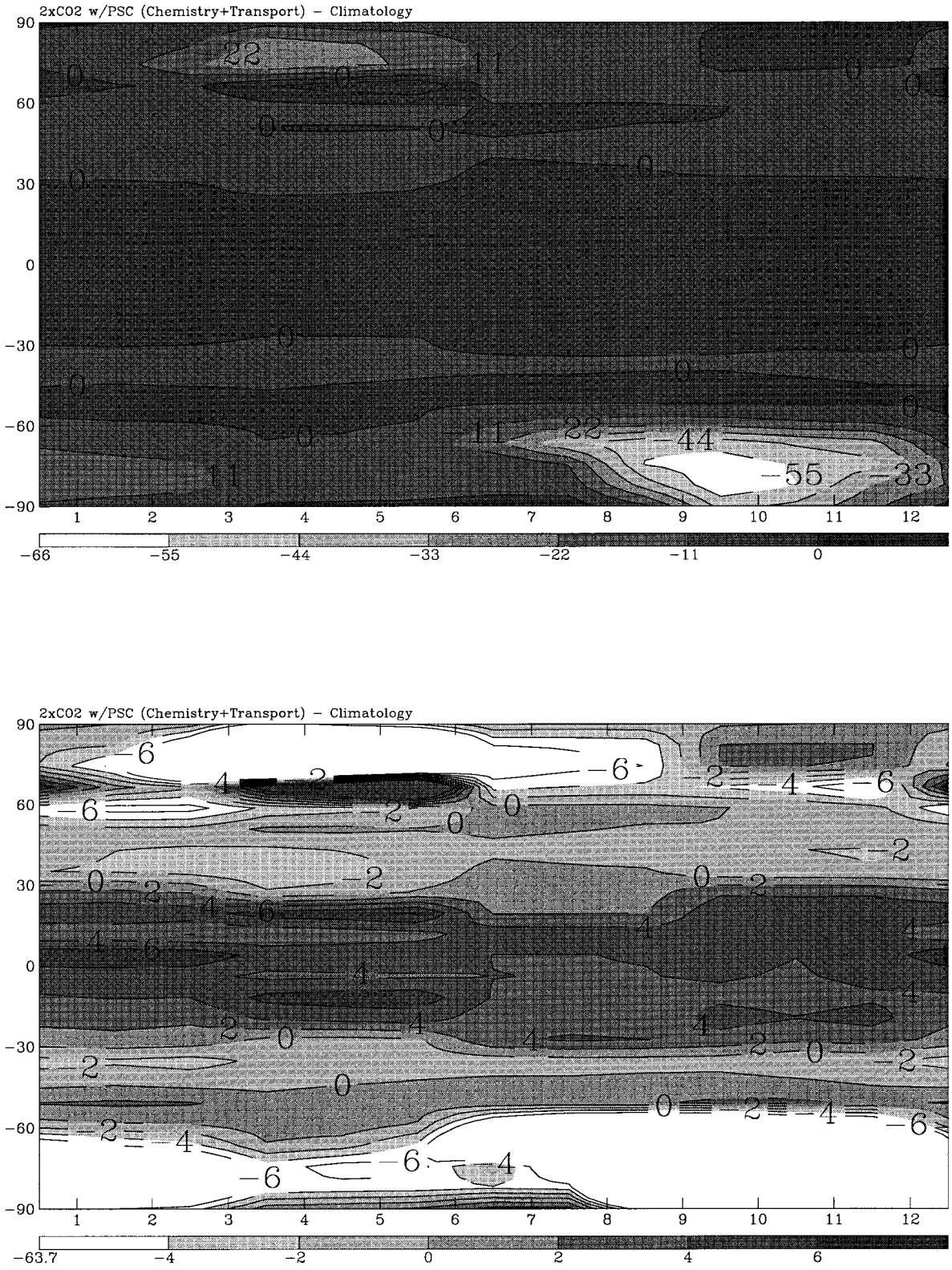

FIG. 15. Change in total column ozone due to doubling of CO_2 as in Fig. 6 but including both photochemical and transport responses.

ferences in the radiation field, which in turn modify the ozone distribution, was included. These parameterizations were incorporated on-line in the GISS GCM, a full-climate model containing detailed radiation and dynamics. The resulting coupled model has been run for 50 yr to allow sea surface temperatures to equilibrate with doubled atmospheric CO_2. We have validated our parameterizations by comparison with the results of previous experiments using stratospheric chemistry models. Additionally, we have calculated off-line the ozone response to changes in diabatic circulation induced by the CO_2 doubling and added these transport changes to the on-line chemical changes. Ozone column increases of ~2%–6% occur in the GCM at equatorial latitudes. These increases are similar to those found in the earlier models that had similar temperature responses to 2 × CO_2 in that region. At middle and high latitudes, however, the ozone response in the GCM is quite different than that found in other models. We calculate an upper tropospheric warming of up to 12°C, while the other models used much smaller-prescribed values. There are significant uncertainties in the determination of both the magnitude and latitude characteristics of the tropospheric warming, but it is clear that this warming has a significant influence on the stratosphere. This large tropospheric warming alters the residual circulation, leading to increased dynamical heating at high latitudes. The warming also extends up into the lower stratosphere at midlatitudes, where higher temperatures increase the reaction rates of ozone depleting chemistry, leading to photochemical ozone losses of up to 7%. We find chemistry plus transport net column ozone decreases of 0%–4% at midlatitudes, in contrast to the increases seen in other models. At high latitudes, we find much smaller ozone increases than the other models as a result of the influence of the tropospheric warming on the model dynamics. When parameterized heterogeneous chemistry on PSCs is included in the GCM, we find a significant vertical, horizontal, and temporal expansion of the Antarctic ozone hole. Furthermore, we find that a significant Arctic ozone hole now forms in the model in four out of five years, with chemistry plus transport column ozone losses averaging about 50% of those in the Antarctic.

Acknowledgments. This work was supported by the NASA Chemistry Modeling and Analysis Program and the NASA Climate Modeling program. D. Shindell was partially supported by a NASA EOS postdoctoral fellowship. Thanks to Jean Lerner for extensive work with graphics programs and to a reviewer for useful comments.

APPENDIX

The Photochemical Model

The 1D photochemical model (Shindell and de Zafra 1996) contains 100 chemical and 31 photolytic reactions and includes the following 39 species: HO_x (H, OH, and HO_2), O_x (O, O^1D, and O_3), NO_x (N, NO, NO_2, and NO_3), Cl_x (Cl, ClO, and OClO), Br_x (Br and BrO), Cl_2, HO_2NO_2, HNO_3, H_2O_2, HCl, N_2O_5, N_2O, HOCl,

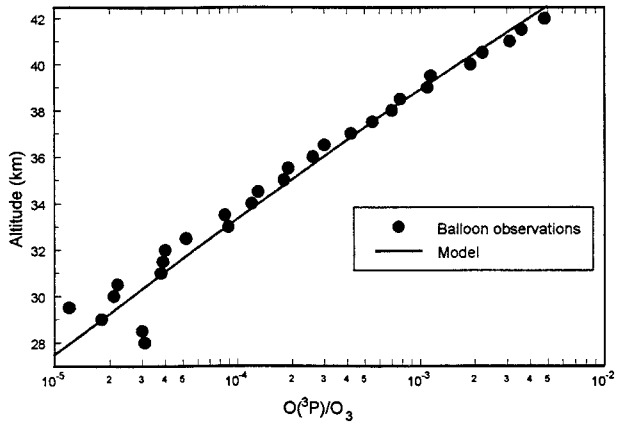

FIG. A1. Observed (Anderson et al. 1980) and modeled O/O_3 ratio at 32°N, 2 December, midday.

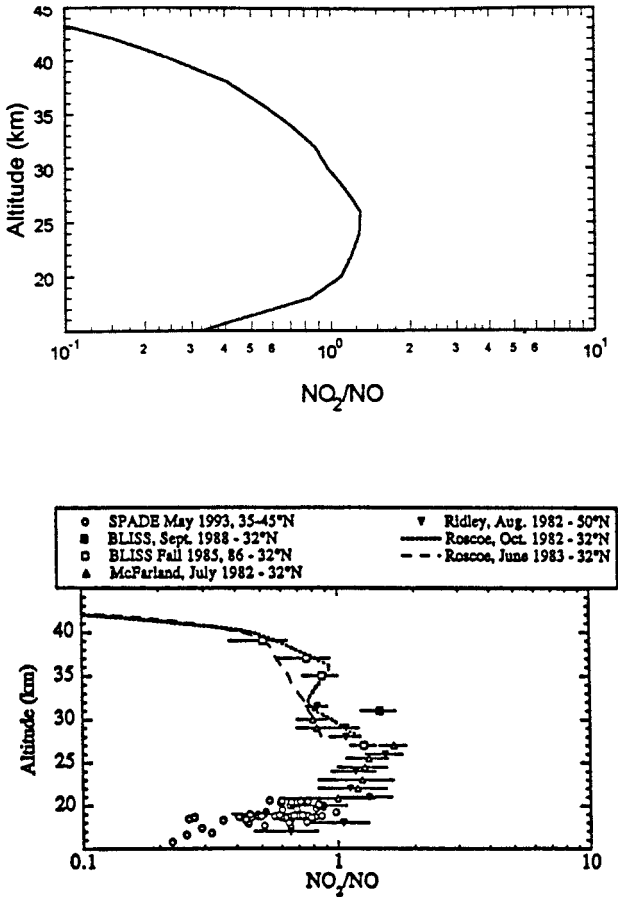

FIG. A2. Modeled NO_2/NO ratio at 32°N, December (upper panel) compared with measured midlatitude ratios (lower panel) as compiled by Jaeglé et al. (1994).

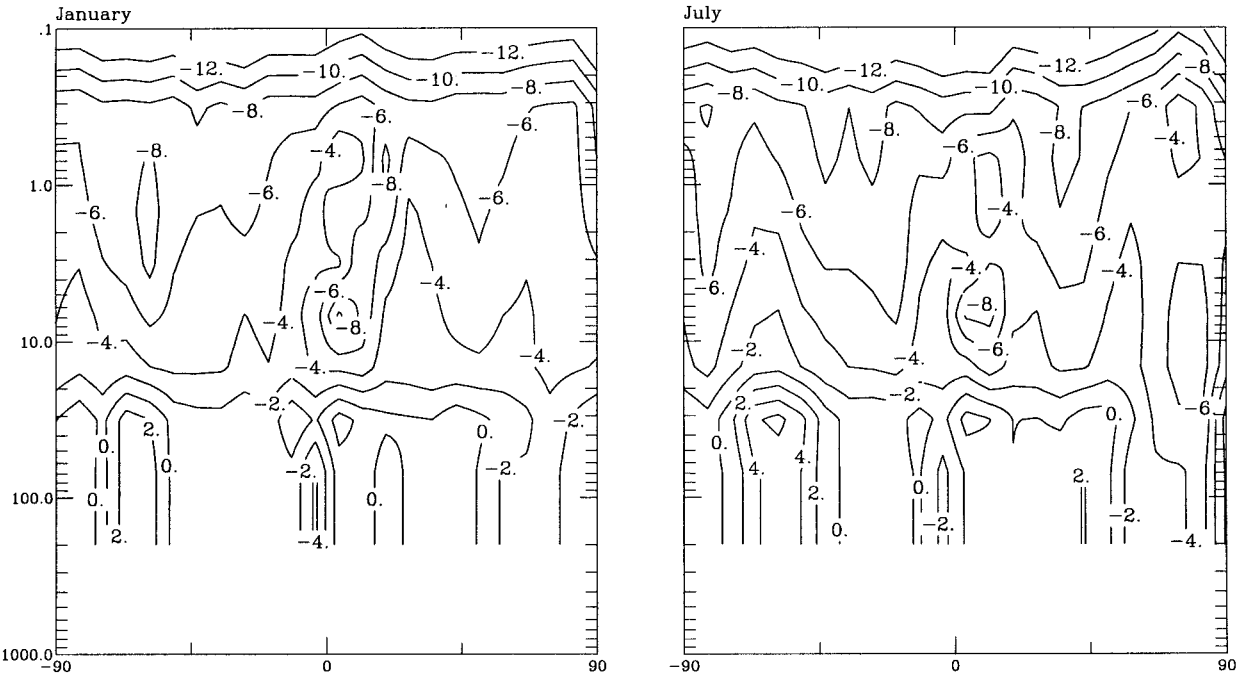

FIG. A3. January and July percentage differences between observed zonal mean ozone (satellite climatology) and quasi-2D modeled values.

$ClONO_2$, H_2O, CH_4, HBr, HOBr, BrCl, $BrONO_2$, CO, Cl_2O_2, $ClNO_2$, H_2, CO_2, CH_3O_2, CH_2O, O_2, and N_2.

Validation of the photolysis scheme is given in Figs. A1 and A2, showing the agreement between the modeled and observed O/O_3 and NO_2/NO ratios. Since odd oxygen chemistry is very rapid, the ratio O/O_3 is almost entirely controlled by oxygen reactions only:

$$\frac{[O]}{[O_3]} = \frac{J_{O_3}}{k_{(0+0_2+M-O_3+M)}[O_2][M]}.$$

This ratio is therefore a good test of the model's ability to correctly calculate the photolysis rate of ozone as a function of altitude. The NO_2/NO ratio is governed by reactions with odd oxygen, odd hydrogen, odd chlorine, and odd bromine, so that validation of the odd nitrogen partitioning is a good indication that at least most of the partitioning of the other reactive families is also correct. As seen in Figs. A1 and A2, the model does a very good job of reproducing the observed ratios.

Figure A3 shows the difference between observed zonal mean ozone (GISS climatology) and modeled values using the quasi 2D approach. The percentage differences in both January and July are quite small, though modeled values tend to be somewhat low above 10 mb, a common phenomenon in photochemical models.

REFERENCES

Anderson, J. G., H. J. Grassl, R. E. Shetter, and J. J. Margitan, 1980: Stratospheric free chlorine measured by balloon-borne in situ resonance fluorescence. *J. Geophys. Res.*, **85,** 2869–2887.

Austin, J., and N. Butchart, 1994: The influence of climate change and the timing of stratospheric warmings on Arctic ozone depletion. *J. Geophys. Res.*, **99,** 1127–1145.

——, ——, and K. Shine, 1992: Possibility of an Arctic ozone hole in a doubled-CO_2 climate. *Nature,* **360,** 221–225.

Brasseur, G., M. H. Hitchman, S. Walters, M. Dymek, E. Falise, and M. Pirre, 1990: An interactive chemical dynamical radiative two-dimensional model of the middle atmosphere. *J. Geophys. Res.*, **95,** 5639–5655.

Cariolle, D. A., A. Lasserre-Bigorry, J. F. Royer, and J. F. Geleyn, 1990: A general circulation model simulation of the springtime Antarctic ozone decrease and its impact on mid-latitudes. *J. Geophys. Res.*, **95,** 1883–1898.

Cubasch, U., K. Hasselmann, H. Hock, E. Maier-Reimer, U. Mikalojewicz, B. Santer, and R. Sausen, 1992: Time-dependent greenhouse warming computations with a coupled ocean–atmosphere model. *Climate Dyn.*, **8,** 55–69.

DeMore, W. B., and Coauthors, 1994: Chemical kinetics and photochemical data for use in stratospheric modeling. Jet Propulsion Laboratory Evaluation 11, 273 pp.

Fels, S. B., J. D. Mahlman, M. D. Schwarzkopf, and R. W. Sinclair, 1980: Stratospheric sensitivity to perturbations in ozone and carbon dioxide: Radiative and dynamical response. *J. Atmos. Sci.*, **37,** 2265–2297.

Intergovernmental Panel on Climate Change, 1995: *Climate Change 1995.* Cambridge University Press, 572 pp.

Jaeglé, L., and Coauthors, 1994: In situ measurements of the NO_2/NO ratio for testing atmospheric photochemical models. *Geophys. Res. Lett.*, **21,** 2555–2558.

Keeling, C. D., R. B. Bacastow, A. F. Carter, S. C. Piper, T. P. Whorf, M. Heimann, W. G. Mook, and H. Roeloffzen, 1989: A three-dimensional model of atmospheric CO_2 transport based on observed winds: I. Analysis of observational data. *Aspects of Climate Variability in the Pacific and the Western Americas, Geophys. Monogr.*, No. 55, Amer. Geophys. Union, 165–236.

Kiehl, J. T., B. A. Boville, and B. P. Briegleb, 1988: Response of a general circulation model to a prescribed Antarctic ozone hole. *Nature,* **332,** 501–504.

Mahfouf, J. F., D. Cariolle, J. F. Royer, J.-F. Geleyn, and B. Timbal, 1994: Response of the Météo-France climate model to changes in CO_2 and sea surface temperature. *Climate Dyn.,* **9,** 345–362.

Mahlman, J. D., J. P. Pinto, and L. J. Umscheid, 1994: Transport, radiative, and dynamical effects of the Antarctic ozone hole: A GFDL ''SKYHI'' model experiment. *J. Atmos. Sci.,* **51,** 489–508.

Manabe, S., and R. T. Wetherald, 1975: The effects of doubling the CO_2 concentration on the climate of a general circulation model. *J. Atmos. Sci.,* **32,** 3–15.

Perliski, L. M., S. Solomon, and J. London, 1989: On the interpretation of seasonal variations of stratospheric ozone. *Planet. Space Sci.,* **37,** 1527–1538.

Pitari, G., S. Palermi, G. Visconti, and R. G. Prinn, 1992: Ozone response to a CO_2 doubling: Results from a stratospheric circulation model with heterogeneous chemistry. *J. Geophys. Res.,* **97,** 5953–5962.

Rind, D., 1987: The doubled CO_2 climate: Impact of the sea surface temperature gradient. *J. Atmos. Sci.,* **44,** 3235–3268.

——, R. Suozzo, N. K. Balachandran, A. Lacis, and G. Russell, 1988a: The GISS global climate/middle atmosphere model. Part I: Model structure and climatology. *J. Atmos. Sci.,* **45,** 329–370.

——, ——, and ——, 1988b: The GISS global climate/middle atmosphere model. Part II: Model variability due to interactions between planetary waves, the mean circulation, and gravity wave drag. *J. Atmos. Sci.,* **45,** 371–386.

——, ——, ——, and M. J. Prather, 1990: Climate change and the middle atmosphere. Part I: The doubled CO_2 climate. *J. Atmos. Sci.,* **47,** 475–494.

——, D. Shindell, P. Lonergan, and N. K. Balachandran, 1998: Climate change and the middle atmosphere. Part III: The doubled CO_2 climate revisited. *J. Climate,* **11,** 876–894.

Roche, A. E., and Coauthors, 1994: Observations of lower-stratospheric ClONO2, HNO_3, and aerosol by the *UARS* CLAES experiment between January 1992 and April 1993. *J. Atmos. Sci.,* **51,** 2877–2902.

Rosenfield, J. E., 1993: Radiative feedback of polar stratospheric clouds on Antarctic temperatures. *Geophys. Res. Lett.,* **20,** 1195–1198.

Schneider, H. R., M. K. W. Ko, R. Shia, and N. Sze, 1993: A two-dimensional model with coupled dynamics, radiative transfer, and photochemistry 2. Assessment of the response of stratospheric ozone to increased levels of CO_2, N_2O, CH_4, and CFC. *J. Geophys. Res.,* **98,** 20 441–20 449.

Shindell, D. T., and R. L. de Zafra, 1996: Chlorine monoxide in the Antarctic spring vortex 2. A comparison of measured and modeled diurnal cycling over McMurdo Station, 1993. *J. Geophys. Res.,* **101,** 1475–1487.

——, and ——, 1997: Limits on heterogeneous processing in the Antarctic spring vortex from a comparison of measured and modeled chlorine. *J. Geophys. Res.,* **102,** 1441–1449.

——, S. Wong, and D. Rind, 1997: Interannual variability of the Antarctic ozone hole in a GCM. Part I: The influence of tropospheric wave variability. *J. Atmos. Sci.,* **54,** 2308–2319.

von Clarmann, T., and Coauthors, 1995: Determination of the stratospheric chlorine budget in the spring arctic vortex from MIPAS B limb emission spectra and air sampling experiments. *J. Geophys. Res.,* **100,** 13 979–13 997.

Woodbridge, E. L., and Coauthors, 1995: Estimates of total organic and inorganic chlorine in the lower stratosphere from in situ and flask measurements during AASE II. *J. Geophys. Res.,* **100,** 3057–3064.

World Meteorological Organization, 1985: Atmospheric ozone. WMO Rep. 16, Global Ozone Res. and Monit. Proj., 614 pp.